Pat1 promotes processing body assembly by enhancing the phase separation of the DEAD-box ATPase Dhh1 and RNA

Ruchika Sachdev[1], Maria Hondele[1], Miriam Linsenmeier[1], Pascal Vallotton[1], Christopher F. Mugler[1,2,3], Paolo Arosio[1], and Karsten Weis [1, 4]

[1] ETH Zurich, 8093 Zurich, Switzerland

[2] University of California, Berkeley, Berkeley CA, 94720, USA

[3] Current address: Amyris Inc. 5885 Hollis Street, Emeryville, 94608, California, USA

[4] To whom correspondence should be addressed

Email: karsten.weis@bc.biol.ethz.ch

Competing interests:

The authors have declared that no competing interests exist.

Abstract

Processing bodies (PBs) are cytoplasmic mRNP granules that assemble via liquid-liquid phase separation and are implicated in the decay or storage of mRNAs. How PB assembly is regulated in cells remains unclear. We recently identified the ATPase activity of the DEAD-box protein Dhh1 as a key regulator of PB dynamics and demonstrated that Not1, an activator of the Dhh1 ATPase and member of the CCR4-NOT deadenylase complex inhibits PB assembly *in vivo* [Mugler et al., 2016]. Here, we show that the PB component Pat1 antagonizes Not1 and promotes PB assembly via its direct interaction with Dhh1. Intriguingly, *in vivo* PB dynamics can be recapitulated *in vitro*, since Pat1 enhances the phase separation of Dhh1 and RNA into liquid droplets, whereas Not1 reverses Pat1-Dhh1-RNA condensation. Overall, our results uncover a function of Pat1 in promoting the multimerization of Dhh1 on mRNA, thereby aiding the assembly of large multivalent mRNP granules that are PBs.

Introduction

Cells are often subjected to severe environmental fluctuations such as nutrient deficiency, temperature changes or osmotic shock. To cope with stresses, a variety of mechanisms have evolved allowing cells to respond acutely and survive. These include changes in the gene expression program, which are often driven by robust transcriptional responses. Yet cells must also inactivate old mRNAs that may interfere with adaptation to the new condition, and therefore, post-transcriptional regulation and RNA turnover are critical to enable rapid changes in gene expression (Ashe et al., 2000; Mager and Ferreira, 1993).

The post-transcriptional fate of eukaryotic mRNAs is tightly linked to the complement of proteins that associate with it to form mRNPs (messenger ribonucleoproteins). For example, the presence of the m^7 G cap structure at the 5' end is crucial for eIF4E binding, while Pab1 binds the 3' poly-A tail, both of which protect the mRNA against degradation and promote translation initiation. On the other hand, mRNA turnover is thought to initiate via deadenylation by the Ccr4/Pop2/Not1 complex (Muhlrad and

46 Parker 1992; Meyer et al., 2004; Sheth and Parker, 2004), followed by cap removal by the decapping
47 enzyme Dcp1/2 and 5'-3' degradation of the transcript by the exonuclease Xrn1 (Coller and Parker
48 2004; Larimer and Stevens, 1990). Thus, the processes of mRNA translation and decay are coupled and
49 act antagonistically (Radakrishnan et al., 2016; Beelman and Parker, 1994; Schwartz and Parker, 1999;
50 Schwartz and Parker, 2000; Sun et al,. 2012; Hu et al., 2009; Chan et al., 2018)

51 The balance between mRNA translation and decay is not only temporally but also spatially controlled.
52 For instance in yeast, upon glucose starvation, the majority of cellular translation halts and
53 untranslated mRNA as well as many factors of the RNA decay machinery concentrate in large
54 cytoplasmic mRNP granules, so called processing bodies [PBs] (Brengues et al., 2005; Sheth and Parker,
55 2003; Teixeira et al., 2005). PBs contain major components of the 5'-3' RNA decay pathway, e.g. Dcp1/2
56 and Xrn1, as well as activators of decapping - namely, the DEAD-box ATPase Dhh1, Pat1, Edc3 and the
57 Lsm1-7 complex. PBs presumably form around mRNAs sequestered away from active translation, and
58 in support of this, inhibition of translation initiation leads to induction of PBs (Frank and Anderson,
59 2008; Chan et al., 2018; Teixeira et al., 2005; Lui et al., 2010). On the contrary, inhibition of translation
60 elongation, for example by the drug cycloheximide which traps mRNA on ribosomes, and prevents
61 their influx into PBs, has the opposite effect and leads to PB disassembly (Texeria et al., 2005; Mugler
62 et al., 2016).

63 In consequence, PBs have been implicated in a variety of post-transcriptional processes such as
64 translational repression (Holmes et al., 2004; Coller and Parker, 2005), mRNA decay (Sheth and Parker,
65 2003; Cougot et al., 2004; Mugler et al., 2016), mRNA storage (Brengues et al., 2005; Bhattacharya et
66 al., 2006), and in higher eukaryotes, micro RNA-mediated repression (Liu et al., 2005; Pillai et al., 2005).
67 PBs and related mRNP granules such as stress granules, P granules in germ cells, neuronal granules etc.
68 form in a number of different species from yeast to mammals, and in a variety of cell types and
69 biological contexts, suggesting that these structures are crucial for cellular function or survival (Barbee
70 et al., 2006; Seydoux and Braun, 2006). Indeed, there is evidence that PBs can be essential for cell
71 survival under stress. For instance, cells unable to form PBs show a drastic loss in viability in stationary

72 phase (Ramachandran et al., 2011; Shah et al., 2013). However, the precise role of PBs in the regulation
73 of gene expression is a matter of debate and in order to understand PB function it is critical to examine
74 how PBs assemble and are regulated.

75 Numerous recent studies have shown that PBs are dynamic, membraneless organelles that assemble
76 from a variety of multivalent but weak RNA-protein, protein-protein and RNA-RNA interactions; a
77 phenomenon called liquid-liquid phase separation [LLPS]. The resulting granules are liquid-like,
78 spherical, dynamic and are dissolved by the alcohol 1,6-hexanediol, all key features of LLPS (Decker et
79 al., 2007; Fromm et al., 2012, 2014; Guo and Shorter, 2015; Mugler et al., 2016; Kroschwald et al.,
80 2015).

81 Although PB formation occurs via a plethora of multivalent protein-RNA interactions in a redundant
82 fashion (Rao and Parker, 2017), there are key players whose deletion drastically attenuates PB
83 assembly (Decker et al., 2007; Pilkington and Parker, 2007; Scheller et al., 2007). One such component
84 is the highly abundant DEAD-box ATPase Dhh1 (DDX6 in humans). Dhh1 is an enhancer of decapping
85 and is involved in the translational repression of mRNAs (Carroll et al., 2011; Coller and Parker,
86 2005; Fischer and Weis, 2002, Coller and Parker 2001). We recently showed that Dhh1 undergoes
87 phase separation *in vitro*, and controls PB dynamics *in vivo* via its RNA-stimulated ATPase activity
88 whereas the ATPase activator Not1 dissolves Dhh1 droplets *in vitro* and inhibits PB formation *in vivo.*
89 However, whether additional factors assist Dhh1 in promoting PB formation remains to be determined
90 and is the focus of this study.

91 One such candidate is the eukaryotic PB component Pat1, an evolutionarily conserved multi-domain
92 RNA binding protein that, like Dhh1, functions in both translational repression and mRNA decay
93 (Pilkington and Parker, 2008; Teixeira and Parker, 2007). In yeast, Pat1 acts as a scaffold that brings
94 together repression and decay factors (Dhh1, Edc3, Lsm1-7, Dcp1/2 etc.) via direct and/or indirect
95 interactions with mRNPs (Nissan et al., 2010). Dhh1 for example directly binds acidic residues in the N-
96 terminal domain of Pat1, an interaction that is conserved across species (Sharif et al., 2013; Conti;

97 Ozgur and Stoecklin, 2013). Deletion of *PAT1* in yeast alters the localization of PB components, whereas
98 its overexpression induces the formation of constitutive PBs even in unstressed cells (Pilkington and
99 Parker, 2007; Coller and Parker, 2005). Furthermore, it was shown that phosphorylation of Pat1 by the
100 cAMP-dependent protein kinase A (PKA) inhibits PB formation, and cells expressing a phospho-mimetic
101 mutant of Pat1 are defective in PB assembly (Ramachandran et al., 2011). However, the mechanism
102 by which Pat1 regulates PB assembly is unclear.

103 Here, we demonstrate that Pat1 promotes PB formation via Dhh1, and we show that the interaction
104 between Pat1 and Dhh1 is critical for robust PB assembly *in vivo*. Using a liquid phase separation assay
105 we can recapitulate this function of Pat1 *in vitro* as addition of recombinant Pat1, but not of a Pat1
106 variant that cannot bind Dhh1, enhances phase separation of Dhh1 and RNA. Overall, our *in vivo* and
107 *in vitro* data suggests that during stress Pat1 antagonizes the inhibitory effect of Not1 on PB assembly
108 and promotes the multimerization of Dhh1 on mRNA, leading to the formation of PBs.

109 **Results**

110 **Constitutive PB formation upon Pat1 overexpression is Dhh1 dependent**

111 The PB components Pat1 and Dhh1 were each previously shown to be required for PB formation in
112 yeast (Pilkington and Parker, 2008; Ramachandran et al., 2011; Mugler et al., 2016; Rao et al., 2017).
113 To understand the relationship between Pat1 and Dhh1 in the regulation of PB assembly, we took
114 advantage of the observation that overexpression of Pat1 leads to constitutive PB formation (Coller
115 and Parker 2005). This allowed us to characterize their respective regulatory contributions without
116 external influences such as nutrient starvation signals. As expected, Pat1 overexpression from its
117 endogenous locus using the galactose promoter in the presence of Dhh1 led to the formation of
118 constitutive PBs, as visualized by co-localization of Dhh1-GFP and Dcp2-mCherry foci (Figure 1A). No
119 foci were formed when Pat1 was not overexpressed or when we overexpressed the human influenza
120 hemagglutinin (HA) tag alone (Figure S1A). Notably, when Pat1 was overexpressed in cells that lack
121 Dhh1, a drastic reduction in the number of PBs was observed, as visualized by the *bona fide* PB marker

122 Edc3-GFP and its co-localization with Dcp2-mCherry (Figure 1 A, B). This demonstrates that formation
123 of constitutive PBs upon Pat1 overexpression requires Dhh1.

124 **Pat1 and Dhh1 interaction is essential for PB assembly**

125 Pat1 is an 88 kDa protein that consists of an N-terminal un-structured domain (Pat1-N) followed by a
126 proline-rich stretch plus middle domain and a C-terminal globular fold (Pat1-C). The N-terminal domain
127 of Pat1 directly binds Dhh1's RecA2 core via a conserved DETF motif (Sharif et al., 2013; Ozgur and
128 Stoecklin, 2013). Furthermore, Pat1's C-terminus harbors two serine residues that are phosphorylated
129 by the cAMP-dependent protein kinase A (PKA) negatively regulating the interaction with Dhh1 and PB
130 formation (Ramachandran et al., 2011).

131 In order to understand how these Pat1 domains influence liquid-liquid phase separation and PB
132 assembly, we wanted to characterize various Pat1 mutants both *in vivo* and *in vitro*. Unfortunately, we
133 were unable to recombinantly express functional, full-length Pat1. Based on the structures published,
134 we therefore developed a minimal Pat1 construct encompassing both N- and C-terminal domains that
135 we refer to as Pat1-NC [amino acids: 5-79 (N) and 456-787 (C) connected with a $(GGS)_4$ linker](Figure
136 1C). The expression of this *PAT1-NC* construct rescued the *pat1Δ* growth phenotype (Figure S1B) and
137 upon glucose starvation, induced PBs to a similar level as wild-type *PAT1* (Figure 1D, E) indicating full
138 functionality *in vivo*. Furthermore, upon re-addition of glucose, PBs in the *PAT1-NC* expressing cells
139 rapidly dissolved demonstrating that they are reversible and dynamic rather than anomalous granules.
140 In addition, Pat1-NC-GFP itself localized to PBs upon stress in a reversible manner (Figure S1C). Finally,
141 when we overexpressed Pat1-NC using a GAL promoter, robust PBs were induced in the absence of
142 stress (Figure 1F, G).

143 We next examined whether Pat1-NC can interact with Dhh1 *in vitro*, and as expected, Pat1-NC
144 displayed strong binding to full-length Dhh1 in a GST pull down assay (Figure 2A). However, this
145 interaction was completely abolished for a Pat1-NC variant in which the N-terminal DETF motif was

146 mutated to four alanines [Pat1$^{4A\text{-}Dhh1}$, see supplemental table S2B for a list of all mutants used in this
147 study] (Figure 2A).

148 We next investigated the effect of the *pat1$^{4A\text{-}Dhh1}$* mutant in the context of the full-length protein on
149 PB formation *in vivo*. While cells expressing *pat1$^{4A\text{-}Dhh1}$* showed a mild growth defect compared to the
150 wild type *PAT1*, they grew significantly better than *pat1Δ* cells, indicating that this protein is at least
151 partially functional (Figure S2A). To examine whether the interaction between Pat1 and Dhh1 is
152 required for PB formation, we monitored PB assembly upon stress in the absence of glucose in wild-
153 type (*PAT1*) or the *pat1$^{4A\text{-}Dhh1}$* background. As expected, the number of PBs was drastically reduced in
154 the complete absence of Pat1, as visualized by Dhh1-GFP (Figure S2B). Importantly, *pat1$^{4A\text{-}Dhh1}$*
155 expressing cells also demonstrated a drastic reduction in PB number compared to cells expressing *PAT1*
156 (Figure 2B, C) and the Pat1$^{4A\text{-}Dhh1}$-GFP protein itself showed a significant defect in localizing to PBs
157 (Figure 2D, E).

158 We were unable to overexpress the *Pat1$^{4A\text{-}Dhh1}$* mutant in yeast. In order to investigate PB formation
159 independently of carbon starvation stress, we therefore treated cells with the drug hippuristanol,
160 which inhibits the eukaryotic translation initiation factor eIF4A (Bordeleau, M.E., et al., 2006). In
161 consequence, hippuristanol prevents translation initiation and robustly induces PB formation within
162 minutes in cells expressing wild-type *PAT1* (Chan et al., 2018) [Figure 2F, Movies 1 and 2]. Cells
163 expressing *pat1$^{4A\text{-}Dhh1}$* however, did not show PB formation until 2hrs after hippuristanol addition.
164 Taken together, our data reveal that direct binding of Pat1 to Dhh1 is required for robust PB assembly.

165 **Pat1 phosphorylation status influences RNA binding**

166 Pat1 is a target of the cAMP-dependent protein kinase A (PKA) and phosphorylation of two serines
167 (amino acids 456/457) in the C-terminus of Pat1 under glucose-rich conditions was previously shown
168 to negatively regulate PB formation (Ramachandran et al., 2011). To better understand how Pat1
169 phosphorylation controls PB assembly, we sought to characterize the influence of the phosphorylation
170 status of Pat1 on PB formation in the absence of additional stresses. Overexpression of *PAT1$^{WT/SS}$* (WT=

171 wild-type) and *pat1*^{AA} (non-phosphorylatable) led to constitutive PB formation as visualized by Dhh1-
172 GFP and Dcp2-mCherry positive foci. However, upon overexpression of *pat1*^{EE} (phospho-mimic), foci
173 number was reduced (Figure 3 A, B). Cells expressing the *pat1*^{EE} mutant also showed a defect in PB
174 formation upon stress in agreement with published literature (Figure S3 A, B and Ramachandran et al.,
175 2011).

176 Pull-down experiments from cell extracts previously suggested that PKA-dependent phosphorylation
177 of Pat1 diminishes its interaction with Dhh1 (Ramachandran et al., 2011). To test whether this effect
178 is direct, we performed pull-down assays with recombinant Pat1-NC protein and the Pat1-NC^{EE} variant.
179 However, in this assay there was no significant difference in Dhh1 binding between Pat1-NC and Pat1-
180 NC^{EE} (Figure 2A). Since the strong DETF binding site in Pat1-N might mask any weaker interaction in
181 Pat1-C, we also tested for direct binding of Pat1-C to Dhh1 but were unable to detect any interaction
182 (Figure 3C), indicating that the DETF-motif in Pat1-N provides the major interaction surface for Dhh1.

183 Pat1-C was previously shown to bind RNA (Pilkington and Parker, 2008; Chowdhury et al., 2014). We
184 therefore tested whether RNA binding is regulated by PKA-dependent phoshphorylation by performing
185 RNA oligo gel shift assays using recombinant proteins. Whereas wild-type Pat1-C robustly binds the
186 RNA oligo and shifts it to higher molecular weight in a native PAGE gel, Pat1^{EE} displayed a significantly
187 reduced RNA shift (quantified in Figure 3D). Taken together, our *in vivo* and *in vitro* results on the
188 phospho-mimic Pat1^{EE} mutant suggest that in addition to Pat1-Dhh1 binding, also the interaction
189 between Pat1 and RNA is important for PB formation.

190 **Pat1 and Not1 act antagonistically *in vivo***

191 Our lab previously showed that Not1 promotes PB disassembly by activating the ATPase activity of
192 Dhh1, and cells expressing a Not1 mutant that cannot bind to Dhh1 (*not1*$^{9X\text{-}Dhh1}$) form constitutive PBs
193 in non-stressed cells. Yet these PBs are less intense and fewer in number than those formed upon
194 glucose starvation (Mugler et al., 2016), indicating that additional mechanisms prevent PB formation
195 in glucose-replete conditions.

196 Since in glucose-rich media PB assembly is also inhibited by the PKA-dependent phosphorylation of
197 Pat1 (Ramachandran et al., 2011), we wanted to test whether expression of the non-phosphorylatable
198 *pat1*^{AA} variant enhances PB formation in the *not1*$^{9X\text{-}Dhh1}$ strain background. While expression of *pat1*^{AA}
199 alone was not sufficient to induce constitutive PBs as observed before (Ramachandran et al., 2011 and
200 Figure 4 A, B), expression of *pat1*^{AA} on top of *not1*$^{9X\text{-}Dhh1}$ significantly increased the number of
201 constitutive PBs compared to cells expressing *not1*$^{9X\text{-}Dhh1}$ alone (Figure 4 A and B). Yet, these PBs are
202 still not as bright and numerous as in stressed wild-type cells. Interestingly, PB intensity strongly
203 increased when these strains were further treated with hippuristanol, a drug that blocks initiation and
204 liberates mRNA molecules from polysomes. The percentage of large PBs was highest in the *pat1*^{AA} *+*
205 *not1*$^{9X\text{-}Dhh1}$ strain, followed by the *not1*$^{9X\text{-}Dhh1}$ and then *pat1*^{AA}.

206 Overall, this suggests that there are at least three determinants that act cooperatively to enhance the
207 formation of PBs: (a) direct interactions between Pat1-Dhh1 and Pat1-RNA; (b) lack of Not1 binding to
208 Dhh1 and in consequence low Dhh1 ATPase activity (Mugler et al., 2016); and (c) the availability of PB
209 client mRNAs that are not engaged in translation. Furthermore, our results suggest that Pat1 and Not1
210 act antagonistically on PB dynamics. Whereas Pat1 binding to Dhh1 enhances the assembly of PBs, the
211 interaction of Not1 with Dhh1 promotes PB disassembly, likely through activation of the ATPase
212 activity of Dhh1.

213 **Pat1 promotes PB assembly by enhancing the phase separation of Dhh1 and RNA**

214 At least two mechanisms of how Pat1 promotes PB formation via Dhh1 could be envisioned: first, Pat1
215 could slow the ATPase cycle of Dhh1, for example by preventing Not1 binding and/or inhibiting ATP
216 hydrolysis, second, Pat1 could directly promote oligomerization and condensation of Dhh1 on RNA.

217 To test the first hypothesis, we used an *in vitro* ATPase assay using purified protein components in
218 which Not1 robustly stimulates the ATPase activity of Dhh1 (Mugler et al., 2016). However, we did not
219 observe a significant inhibition of the Not1-stimulated ATPase activity upon addition of Pat1-NC (Figure
220 S4A), suggesting that Pat1 does not directly interfere with the mechanism of ATPase activation.

221 We had previously shown that PB dynamics are regulated by the ATPase activity of Dhh1 (Carroll et al.,
222 2011; Mugler et al., 2016). To test Pat1's effect on the Dhh1 ATPase cycle *in vivo,* we therefore also
223 examined the turnover of PBs that form upon Pat1 overexpression. The drug cycloheximide (CHX) traps
224 mRNAs on polysomes and thereby stops the supply of new RNA clients to PBs. Since active Dhh1
225 constantly releases mRNA molecules from PBs, a lack of mRNA influx eventually leads to their
226 disassembly and in consequence the catalytic dead mutant of Dhh1 that is locked in the ATP- state
227 ($Dhh1^{DQAD}$) inhibits PB disassembly and was shown to have negligible turnover rates (Mugler et al.,
228 2016; Kroschwald et al., 2015). We observed that PBs formed upon Pat1 overexpression were more
229 dynamic than PBs formed in the presence of $Dhh1^{DQAD}$ and their dis-assembly kinetics was comparable
230 to PBs formed upon stress in a wild-type *DHH1* background (Figure S4B, C and Movies 3,4,5). Thus,
231 overall, our *in vitro* and *in vivo* findings are not consistent with the conclusion that Pat1 blocks the
232 ATPase activation of Dhh1.

233 The second hypothesis is that Pat1 promotes higher-order mRNP assembly by directly or indirectly
234 promoting Dhh1 oligomerization, thereby acting as a scaffold and providing additional protein-protein
235 or protein-RNA interactions (Coller and Parker, 2005; Roy and Parker, 2017). We have previously
236 shown that recombinant Dhh1 can undergo liquid-liquid phase separation (LLPS) in the presence of
237 RNA and ATP, and that these Dhh1 droplets can recapitulate aspects of *in vivo* PB dynamics. (Mugler
238 et al., 2016). We therefore utilized this *in vitro* system to test Pat1's impact on the phase separation
239 behavior of Dhh1.

240 Dhh1 droplets were assembled from purified components as described previously (Mugler et al.,
241 2016). Interestingly, while no LLPS of Pat1 alone was detected (Figure S5A), addition of increasing
242 concentrations of wild-type Pat1 strongly enhanced the LLPS of Dhh1 in the presence of ATP and RNA
243 as judged by an increase in the area * intensity of Dhh1 droplets (Figure 5A). Furthermore, Pat1 itself
244 enriched in Dhh1 droplets, suggesting that Pat1 and Dhh1 co-oligomerize with RNA to form a
245 composite phase-separated compartment.

246 To test the specificity of LLPS stimulation, we tested the Pat1$^{4A\text{-}Dhh1}$ (Dhh1 binding) and Pat1^{EE} (phospho-
247 mimic) mutants both of which both drastically reduce PB formation *in vivo* (see Figure 2A, 3A and S2B).
248 Consistent with the *in vivo* results, Dhh1-RNA droplet formation was either not at all or only mildly
249 stimulated upon addition of these Pat1 variants (Figure 5A).

250 We previously demonstrated that the MIF4G domain of Not1 prevents formation of Dhh1-RNA
251 droplets, presumably by activating the ATPase cycle of Dhh1 (Mugler et al., 2016). We therefore next
252 analyzed whether the Pat1-Dhh1 droplets are still responsive to Not1. Similar to what we observed *in*
253 *vivo* (Figure 4), Not1^{MIF4G} also diminishes formation Dhh1 droplets in the presence of Pat1 *in vitro*
254 (Figure 5B).

255 Taken together our results suggest that Pat1 enhances the multivalency of protein-protein and
256 protein-RNA interactions in a Dhh1-Pat1 mRNP and in consequence promotes the formation of higher-
257 order, liquid-like mRNP droplets akin to *in vivo* PBs.

258 ***In vitro* phase separated droplets mimic the stoichiometry of PB components *in vivo***

259 To examine how well our *in vitro* droplets resemble *in vivo* PBs we investigated the stoichiometric ratio
260 of Dhh1:Pat1 in these granules. In order to determine the stoichiometry *in vivo,* we measured the
261 number of PBs and the fluorescence intensity of GFP-tagged Dhh1 and Pat1 in these foci. Briefly, we
262 glucose starved both Pat1-GFP and Dhh1-GFP expressing cells to induce PBs (Figure S6A) and used the
263 single particle tracking software Diatrack to count the number and intensity of PBs in an unbiased and
264 automated manner in each strain [Vallotton et al., 2013]. Surprisingly, despite the fact that the cellular
265 concentration of Pat1 is ten-times lower than Dhh1 (Figure S6B), the ratio of the two PB components
266 was approximately 2:1+/-0.18 (Dhh1:Pat1) after 0.5-4 hours of starvation (Figure 6A). Extended
267 starvation resulted in enhanced Dhh1 recruitment to PBs until reaching a Dhh1:Pat1 ratio of 2.5:1+/-
268 0.23, suggesting that PB composition matures over time (Figure 6).

269 In order to determine the stoichiometry of Pat1 and Dhh1 droplets *in vitro*, we imaged Dhh1-mCherry
270 and Pat1-GFP droplets with a confocal microscope (Figure S6C). The protein concentration of both

271 Dhh1 and Pat1 in the droplet was calculated from a standard curve determined from values measured
272 for different concentrations of the respective soluble fluorophores (Figure 6B). Remarkably, we found
273 a stoichiometric ratio of 2.7:1 +/- 0.13 of Dhh1 to Pat1 in the *in vitro* phase-separated droplets, closely
274 resembling the Dhh1:Pat1 ratio of mature PBs *in vivo* (Figure 6B).

275 Thus, while other mRNA decay factors also contribute to PB formation *in vivo*, our data demonstrate
276 that with a minimal number of constituents, namely Dhh1, RNA, ATP and Pat1 higher-order dynamic
277 liquid droplets can be formed *in vitro*. The *in vitro* droplets recapitulate various properties of PBs
278 formed *in vivo* such as (a) the stoichiometry of PB components, and (b) the dynamics of Pat1-
279 stimulated assembly and Not1-stimulated disassembly of *in vivo* PBs identifying Pat1 as an important
280 player in PB formation promoting LLPS via Dhh1.

281

282 **Discussion**

283 **Tug-of-war model between Pat1 and Not1 to regulate PB dynamics**

284 The ability of proteins and RNA to undergo liquid-liquid phase separation (LLPS) has emerged as an
285 essential fundamental biological process allowing cells to organize and concentrate their cellular
286 components without the use of membranes. Yet, how these membraneless organelles assemble, are
287 kept dynamic and are regulated remains enigmatic. One such cellular phase-separated compartment
288 is the PB and our results presented here together with our prior work (Mugler et al., 2016) identify and
289 characterize both positive and negative regulators of PB assembly and provides novel insight into the
290 regulation of membraneless organelle formation.

291 Overall, our work uncovers a function of Pat1 as an enhancer of PB formation that acts via Dhh1 and
292 counteracts the inhibitory function of Not1. Based on our results, we propose that there are at least
293 three inputs that cooperatively regulate PB dynamics *in vivo* (Figure 6C). First, the availability of mRNA
294 clients acting as seeding substrates to initiate PB formation. mRNA availability is inversely proportional
295 to the translation status, which is regulated by different stress responses and the metabolic state of

296 the cell (Figure 2C). Second, the activity of cAMP-dependent PKA negatively regulates PB assembly in
297 nutrient-rich conditions, at least in part through phosphorylation of Pat1. However, since expression
298 of non-phosphorylatable Pat1^{AA} at endogenous levels (in contrast to overexpression) is not sufficient
299 to induce PBs, Pat1 availability appears to be limiting (Figure 6, 3A, S2B and Ramachandran et al.,
300 2011). Third, activation of the Dhh1 ATPase cycle by the CCR4-Not1 deadenylation complex stimulates
301 mRNA release and negatively regulates PB assembly. It is of note that Not1 itself might also be subject
302 to post-translational regulation, in response to metabolic state and/or cell cycle stages of the cell
303 (Mugler et al., 2016; Braun et al., 2014).

304 In this model, a tug-of-war between Pat1 and Not1 regulates PB assembly and disassembly: whereas
305 a tight Pat1-Dhh1 interaction in the presence of RNA clients, promotes PB formation, Not1, induces PB
306 turnover via stimulating the ATPase activity of the DEAD box ATPase Dhh1 (Figure 6C). Remarkably,
307 our *in vivo* findings are corroborated *in vitro* wherein, Pat1 enhances the LLPS of Dhh1 and RNA, a step
308 critical for the assembly of large mRNP granules, and by contrast, Not1 reverses the LLPS of Pat1-Dhh1-
309 RNA droplets (Figure 6, 4, 5B). Furthermore, the observed stoichiometry of Dhh1 and Pat1 in PBs is
310 recapitulated in our *in vitro* phase separation assay.

311 **The interaction between Pat1 and Dhh1 is critical for PB assembly**

312 Inducing PB formation by Pat1 overexpression or hippuristanol treatment allowed us to dissect distinct
313 mechanisms that govern PB assembly and characterize the crucial role of the Pat1-Dhh1 interaction in
314 this process. The benefit of these modes of PB formation are that they bypass the characteristic
315 stresses associated with PB formation, such as nutrient starvation, that might have more widespread
316 and confounding effects on translation, mRNA degradation, or on the regulation of other PB
317 components.

318 Our experiments reveal that Pat1 functions in PB formation through Dhh1 since PB induction by Pat1
319 overexpression is strictly dependent on the presence of Dhh1 (Figure 1A). Furthermore, a mutant in
320 the DETF motif in the N-terminus of Pat1 mediating direct binding to Dhh1 (Pat1$^{4A\text{-}Dhh1}$ variant) fails to

321 promote PB assembly (Figure 2). These results were further confirmed using the drug hippuristanol
322 that inhibits translation initiation wherein PBs were induced in wild-type cells but not in cells
323 expressing the Pat1$^{4A\text{-}Dhh1}$ mutant (Figure 2E, Chan et al., 2018) suggesting that high mRNA load alone
324 is inadequate for PB formation and that a direct physical interaction between Pat1 and Dhh1 is
325 obligatory as well. Since the DETF motif in Pat1 is conserved across evolution and was suggested to
326 regulate PB assembly in human cells as well (Sharif et al., 2013; Ozgur and Stoecklin, 2013), the Pat1-
327 Dhh1 interaction likely plays a critical role in PB formation across species.

328 Our results seem to be at odds with a previous publication, which suggests that Pat1 acts
329 independently of Dhh1 to promote PB formation (Coller and Parker 2005). However, in this study Pat1
330 was overexpressed from a plasmid, on top of the endogenous copy. When recapitulating these
331 conditions, we observed that PB components mislocalize to the nucleus [observed by DAPI and a
332 nuclear rim marker, see Figure S7A, B.] and it is possible that in the absence of additional organelle
333 markers, this nuclear accumulation was misinterpreted as PB formation.

334 **Pat1 enhances the LLPS of Dhh1, thereby promoting PB formation**

335 How does Pat1 enhance PB formation? One hypothesis is that Pat1 directly counteracts the Not1-
336 stimulated ATPase activation of Dhh1, but we do not favor such a model since i) Pat1 does not inhibit
337 Dhh1's ATPase activity at physiological protein ratios *in vitro* (Figure S3A), ii) Not1^{MIF4G} dissolves Pat1-
338 Dhh1 condensates, while droplets formed from catalytic-dead Dhh1^{DQAD} are Not1-resistant (Figure 6
339 and Mugler et al., 2016), and iii) *in vivo*, PBs formed upon Pat1 overexpression are much more dynamic
340 than those formed from Dhh1^{DQAD} (Figure S3B).

341 Instead, our data are consistent with a model in which Pat1 promotes PB assembly by directly
342 enhancing the LLPS of Dhh1. DDX6, the human homolog of Dhh1 can oligomerize (Lange et al., 2012),
343 and given the fact that both DDX6 and Dhh1 are found in molar excess over mRNA, we propose that
344 Pat1 functions as a scaffold, providing additional multivalent interactions with Dhh1 and RNA, thereby
345 aiding in the fusion of Dhh1 LLPS droplets and promoting assembly of microscopically-detectable

346 mRNP condensates (Figure 5). Interestingly, both functional binding to Dhh1 in Pat1-N and RNA-
347 binding in Pat1-C are required for this mechanism as individually mutations in each of the domains
348 alter PB assembly *in vivo* and fail to enhance Dhh1's phase separation *in vitro*. Furthermore, the Pat1^{4A-}
349 ^{Dhh1} (Dhh1 binding mutant) and Pat1^{EE} (phospho mimic mutant) not only have a drastically reduced
350 number of PBs, but also much lower intensity (reduced by 7 and 8 fold respectively, Figure S7C)
351 compared to Pat1 wild-type PBs. It is interesting to note that Pat1-N was previously shown to interfere
352 with the ability of Dhh1 to interact with RNA (Sharif et al., 2013). This might explain why RNA-binding
353 by Pat1's C-terminus that is under the regulation of PKA (Figure 3, S3) is critical for LLPS and PB
354 assembly.

355 Our recent findings also show that the un-structured poly-Q rich C-terminal tail of Dhh1 is required for
356 PB formation *in vivo* and Dhh1 LLPS *in vitro* (Hondele et al., *under revision*). Thus, Pat1 might potentially
357 enhance Dhh1 multimerization via the low complexity tails of Dhh1. Structural studies will now be
358 needed to clarify how Pat1 facilitates oligomerization and PB formation of the Dhh1-Pat1- RNA
359 complex.

360 **The emerging importance of liquid-liquid phase separation in diverse aspects of cell biology and the**
361 **power of *in vitro* reconstitution systems**

362 As non-membrane bound organelles, it is of interest to understand how cells assemble large RNP
363 granules and regulate their dynamics. PBs are prominent membraneless cellular compartments, which
364 have been shown to be not only involved in numerous aspects of mRNA turnover, but also crucial for
365 survival under various cellular stresses. With an *in vitro* phase separation tool in hand that faithfully
366 reconstitutes certain aspects of PB formation, we are now in a position to dissect how PBs form and
367 characterize their biophysical behavior. This will aid us not only in elucidating key components of PB
368 formation, but also help us elucidate the function of PBs in regulating mRNA turn-over. At this stage,
369 our in *vitro* systems are limited to Dhh1, Pat1, Not1 and RNA and it must be pointed out that several
370 additional PB components have been characterized. It will thus be critical to examine also these

371 components in future experiments and to evaluate their role in PB dynamics and how they function
372 together with Pat1 and Dhh1. For example, this includes the low complexity-domain containing factors
373 Edc3 and Lsm4 that were shown to be critical for PB formation *in vivo.* Recently, it was demonstrated
374 that in addition to regulatory inputs through signaling pathways a threshold concentration of low-
375 complexity domain containing proteins is required for robust PB assembly (Protter et al., 2018). In the
376 future, it will thus be important to evaluate the effect of concentration thresholds on Dhh1-based LLPS
377 *in vitro* and PB formation *in vivo* to understand the complex interplay of various inputs that regulate
378 PB assembly.

379 The physical basis of LLPS has attracted a great deal of attention recently, at least in part because of
380 the critical role that proper mRNP assembly plays in pathological neurodegenerative diseases and
381 stress responses (Ramaswami et al., 2013; Alberti and Hyman 2016; Patel et al., 2015; Aguzzi and
382 Altmeyer, 2016; Hyman et al., 2014). An important challenge is to understand how these granules are
383 kept dynamic and functional under some conditions whereas the formation of solidified and aberrant
384 aggregates are triggered under others. Robust *in vitro* reconstitution systems that can recapitulate
385 mRNP granule assembly, dynamics and stoichiometry will be invaluable in addressing these research
386 questions and increase our understanding of the molecular mechanism of how cells age and deal with
387 stress.

388

389 **Materials and methods**

390 **Construction of yeast strains and plasmids**

391 *S. cerevisiae* strains used in this study are derivatives of W303 and are described in table S1. ORF
392 deletion strains and C-terminal epitope tagging of ORFs was done by PCR-based homologous
393 recombination, as previously described (Longtine et al., 1998). Plasmids for this study are described
394 in table S2A. Mutations in Pat1 were generated by introducing the mutation in the primer used to
395 amplify the respective Pat1 regions and stitched together with the selection marker from the plasmid

396 (table S2B). Mutations in Dhh1 and Not1 were generated as in Mugler et al., 2016. Primer sequences
397 for strain construction are listed in table S2C.

398 **Overexpression of Pat1 wild-type and mutants**

399 The samples were grown overnight in synthetic media containing 2% raffinose, diluted to OD_{600} = 0.05
400 or 0.1 the following day, and grown to mid-log phase (OD_{600}= 0.3–0.4). The culture was split into two
401 and to one-half galactose was added to 2% final concentration and the corresponding protein induced
402 for 2-3 hours. The cells in both raffinose and galactose were imaged using a wide-field fluorescence
403 microscope.

404 **PB induction and disassembly kinetics**

405 PBs were induced via glucose starvation stress. Samples were grown overnight in synthetic media
406 containing 2% glucose, diluted to OD_{600} = 0.05 or 0.1 the following day, and grown to mid-log phase
407 (OD_{600}= 0.3–0.8). Cells were harvested by centrifugation and washed in ¼ volume of fresh synthetic
408 media +/− 2% glucose, then harvested again and re-suspended in 1 volume of fresh synthetic media
409 +/− 2% glucose and grown 30 min at 30°C. Cells were then transferred onto Concanavalin A-treated
410 MatTek dishes (MatTek Corp., Ashland, MA) and visualized at room temperature. For cycloheximide
411 experiments, final concentration of 50ug/mL (Sigma-Aldrich, CH) were used to examine PB disassembly
412 kinetics. For PB induction and to determine the kinetics of PB assembly we used hippuristanol (a
413 generous gift of Junichi Tanaka, University of the Ryukyus) at a final concentration of 10µM.

414 **Wide-field fluorescence microscopy**

415 Cells were transferred onto Concanavalin A-treated MatTek dishes (MatTek Corp., Ashland, MA) and
416 visualized at room temperature. Microscopy was performed using an inverted epi-fluoresence
417 microscope (Nikon Ti) equipped with a Spectra X LED light source and a Hamamatsu Flash 4.0 sCMOS
418 camera using a 100x Plan-Apo objective NA 1.4 and the NIS Elements software. Representative images
419 were processed using ImageJ software. Brightness and contrast were adjusted to the same values for
420 images belonging to the same experiment and were chosen to cover the whole range of signal

421 intensities. Image processing for PB analysis was performed using Diatrack 3.05 particle tracking
422 software (Vallotton et al., 2013) as described below.

423 **Automated image analysis for PB quantification**

424 In order to quantify PB formation in live cells, we used an automated image analysis in a manner similar
425 to Mugler et al., 2016. First, PBs were counted using Diatrack 3.05 particle tracking software using local
426 intensity maxima detection, followed by particle selection by intensity thresholding and particle
427 selection by contrast thresholding with a value of 5% (Vallotton et al., 2017). To speed up the analysis,
428 we renamed all our images in a form that can be recognized as a time-lapse sequence by Diatrack, and
429 placed them all in a single directory, such that they all will be analyzed using exactly the same image
430 analysis parameters. Renaming and copying was done by a custom script (supplementary code 1),
431 which also performed cell segmentation using a method adapted from (Hadjidemetriou et al., 2014).
432 Briefly, the method first detects all edges using a Laplacian edge detection step, and then traces
433 normals to those edges in a systematic manner. These normals tend to meet at the cell centre where
434 the high density of normals is detected, serving as seeds to reconstruct genuine cells. Our script thus
435 counts cells and reports their number for each image - information which is output to an excel table.
436 The results from Diatrack PB counting are imported from a text file into that table, and the number of
437 PB is divided by the number of cells for each image.

438 **Protein purification**

439 Dhh1 and Not1 were purified as described previously (Mugler et al., 2016). V5-Pat1-C and GST-Pat1-
440 NC constructs as described in Supplementary table S2A were cloned into pETM-CN vectors. These
441 expression vectors were transformed into chemically competent *E. coli* BL21 DE3 under the selection
442 of ampicillin and chloramphenicol. Pre-cultures were grown in LB at 37°C over-night, and diluted 1:100
443 into rich medium the next morning. Cells were grown at 37°C to an OD_{600} of 0.6 and induced with 200
444 mM IPTG (final concentration). Cells were then grown overnight at 18°C, harvested and resuspended
445 in 30 mL lysis buffer (500mM (Pat1-C) or 300 mM NaCl (Pat1-NC), 25 mM Tris-HCl pH 7.5, 10 mM
446 imidazole, protease inhibitors, 10% glycerol) per cell pellet from 2 L of culture. After cell lysis by

447 EmulsiFlex (Avestin Inc, Ottawa, CA), the 6xHis tagged proteins were affinity extracted with Ni^{2+}
448 sepharose in small columns, dialyzed into storage buffer (MH200G (Pat1-C): 200 mM NaCl, 25 mM Tris
449 pH 7.5 (RT), 10% glycerol, 2 mM DTT), MH300G (Pat1-NC): same with 300mM NaCl) with simultaneous
450 protease cleavage of the His-tag and GST-tag (unless required for pull-down assays) and further
451 purified by size exclusion with a Superdex 200 column on an AEKTA purifier (both GE Life Sciences,
452 Marlborough, MA) in storage buffer. Protein expression levels, His eluates and gel filtration fractions
453 were analyzed by SDS-PAGE. Clean Superdex elution fractions were pooled, concentrated using
454 Millipore Amicon Centrifugation units and snap frozen as ~ 20 µl aliquots in siliconized tubes in liquid
455 nitrogen.

456 **ATPase assays**

457 ATPase assays were performed according as described (Montpetit et al., 2011) with the following
458 modifications: final concentration 2 µM Dhh1-mCherry was mixed with 0.5 µM Not1 and Pat1-mCherry
459 (1 and 3µM) as indicated and protein volumes equalized with storage buffer (MH200G). 2 µL 10x
460 ATPase buffer (300 mM HEPES-KOH pH 7.5, 1 M NaCl, 20 mM $MgCl_2$), 4 µL 10 mg/ml polyU (unless
461 indicated otherwise), RNase inhibitors, 13.3 µL 60% glycerol, 2.7 µL 10 mg/mL BSA, were added to a
462 final volume of 36 µL. Reactions were set up in triplicate in a 96-well NUNC plate. The assay was
463 initiated by the addition of 40 µL of a master mix containing 1x ATPase buffer, 2.5 mM ATP (from a
464 100 mM stock in 0.5 M HEPES-KOH pH 7.5), 1 mM DTT, 6 mM phosphoenolpyruvate, 1.2 mM NADH
465 (from a 12 mM stock in 25 mM HEPES-KOH pH 7.5) and 125–250 units / mL PK/LDH. NADH absorption
466 was monitored with a CLARIOstar plate reader (BMG Labtech, Ortenberg, Germany) at 340 nm in 30 s
467 intervals for 400 cycles.

468 ***In vitro* liquid droplet reconstitution assay**

469 Reactions were pipetted in 384-well microscopy plates (Brooks 384 well ClearBottom Matriplate, low
470 glass). Proteins were diluted to 50 µM (Dhh1) or 100 µM (Not1, Pat1) stocks with storage buffer and

471 mixed as droplets at the side of the well; volumes were equalized to 5 µl with storage buffer. Next, a
472 master mix of 12.5 µl 150 mM KCl buffer (150 mM KCl, 30 mM HEPES-KOH pH 7.4, 2 mM $MgCl_2$), 2µl
473 ATP reconstitution mix (40 mM ATP, 40 mM $MgCl_2$, 200 mM creatine phosphate, 70 U/mL creatine
474 kinase), 2.5 µl 2mg/ml polyU (in H_2O) as an RNA analog, 1 µl 1M HEPES-KOH pH 6.4 buffer and 2 ml
475 10mg/ml BSA were added and mixed by pipetting, the droplets still at the side of the well, since this
476 later on produced more equal droplet distribution. First imaging was performed after 20 minutes
477 incubation at room temperature; just prior to imaging, droplets were spun down at 100 g for 1
478 minute. For subsequent analysis, plates were stored in the fridge. Pictures displayed were recorded
479 after 1 hour incubation.

480 **Stoichiometry analysis of Dhh1 and Pat1 in PBs *in vivo***

481 In order to estimate the relative amount of Dhh1 to that of Pat1 in PBs *in vivo*, we labelled both proteins
482 with eYGFP in two separate strains, and imaged them in exactly the same conditions after inducing
483 carbon (glucose) starvation stress for indicated times (Figure 6A). Using exactly the same endogenous
484 probe for both proteins allowed us to deduce ratios of abundances directly from ratios of intensities
485 (no spectral corrections are necessary). We then measured the intensity of the 10 brightest PBs as a
486 function of time and in both cases took the median intensity value as representative of the more visible
487 PBs (at least 10 PBs were present in every image for both strains and at each time point). Finally, we
488 divided the median value obtained for Dhh1 by that for Pat1 and plotted that ratio as a function of
489 time post-stress.

490 **Stoichiometry of Dhh1 and Pat1 in phase-separated *in vitro* droplets**

491 For the analysis of the *in vitro* phase transition of Dhh1 in the presence of Pat1, 2 µM mCherry-tagged
492 Dhh1 and 4 µM GFP-tagged Pat1-NC were added to 0.1 mg/mL polyU and 5 mM ATP in 150 mM KCl,
493 30 mM HEPES-KOH, pH 7.4 and 2 mM $MgCl_2$. After 1 hour incubation, the phase-separated droplets
494 were imaged in both the mCherry and the GFP channel by confocal fluorescence microscopy (Leica TCS
495 SP8) with a 63x NA 1.4 oil objective (Leica). The protein concentration was evaluated from the

496 fluorescence intensity via a standard curve obtained by measuring a series of samples at different
497 known concentrations for each fluorophore. The size distributions were obtained by analyzing the
498 images obtained by fluorescence microscopy with an in-house code written in Matlab.

499 **GST pull-down assays**

500 25 µl of 100 µM recombinant purified GST Pat1-NC was bound to 30 µl GST-slurry (Sigma), and one
501 aliquot of GST-beads was included without added Pat1-NC as negative control. Reactions were
502 incubated for 30mins rotating at 4°C and washed 4-times with wash buffer (300 mM NaCl, 10 mM Tris
503 pH 7.5, 0.05 % NP40). 4 µl 250 µM Dhh1 was added in 500 µl wash buffer and incubated rotating at
504 4°C for 1 hour. Reactions were washed 5-times, proteins eluted by boiling with 4x SDS loading buffer
505 and separated on a 12% acrylamide gel and stained with Coomassie. For V5-pulldown assays, the bait
506 (15 µl 100 µM Pat1-C construct) was bound to 15 ml V5-slurry (Sigma), the bait 3 µl 200 µM Dhh1-
507 mCherry, and incubation / wash buffers as above with salt concentration as indicated in the blot. Final
508 washes were only performed three times.

509 **Native PAGE**

510 Proteins were diluted to 20 µM. 0, 2 or 4 µl of protein solution was filled to 4 µl with storage buffer
511 (200mM NaCl, 25mM Tris pH 7.5, 10% glycerol, 2 mM DTT). Proteins were mixed with a master mix
512 containing per reaction 2 µl 10x ATPase buffer (300 mM HEPES-KOH pH 7.5, 1 M NaCl, 20 mM MgCl2),
513 0.3 µl Cy5-labeled *in vitro* transcribed RNA oligo (29nt, 1.1 µg/µl), 2 µl 2.5M NaCl, 13.7 µl H2O and 3 µl
514 60% glycerol. Reactions were incubated on ice for 20 min and separated on a precast Bis-Tris Native
515 gradient Gel (Invitrogen) in 1x running buffer (50 mM Bis-Tris 50 mM Tricine pH 6.8) at 100V 4C for
516 about 2.5hrs.

517 **Growth curve**

518 Overnight yeast cultures were grown in permissive conditions in SCD media. Growth curves were
519 acquired using CLARIOstar automated plate reader (BMG Labtech, Ortenberg, Germany) at 30°C in 24-

520 well plastic dishes (Thermo Fisher) from overnight pre-cultures diluted 1:125 in the specified synthetic
521 liquid media.

522 **Western blotting**

523 For Western blot analysis, roughly 5 OD_{600} units of log growing cells were harvested and treated with
524 0.1M NaOH for 15 mins at room temperature. The samples were vortexed in between and finally
525 centrifuged to remove the NaOH. SDS sample buffer was added and homogenates were boiled.
526 Proteins were resolved by 4–12% Bolt Bis-Tris SDS PAGE (Thermo Fischer, Waltham, MA), then
527 transferred to nitrocellulose membrane (GE Life Sciences, Marlborough, MA). Membranes were
528 blocked in PBS with 5% non-fat milk, followed by incubation with primary antibody overnight.
529 Membranes were washed four times with PBS with 0.1% Tween-20 (PBS-T) and incubated with
530 secondary antibody for 45 min. Membranes were imaged and protein bands quantified using an
531 infrared imaging system (Odyssey; LI-COR Biosciences, Lincoln, NE). The following primary antibodies
532 were used for detection of tagged proteins at the indicated dilutions: mouse-anti-GFP (1:1000) (Roche
533 Cat# 11814460001, RRID: AB_390913), and rabbit-anti-Hxk1 (1:3000) (US Biological Cat# H2035-01,
534 RRID: AB_2629457, Salem, MA). IRdye 680RD goat-anti-rabbit (LI-COR Biosciences Cat# 926–68071,
535 RRID: AB_10956166) and IRdye 800 donkey-anti-mouse (LI-COR Biosciences Cat# 926–32212, RRID:
536 AB_621847) were used as secondary antibodies.

537

538 **ACKNOWLEDGEMENTS**

539 We would like to thank Justine Kusch and the ETHZ ScopeM facility for technical assistance with
540 confocal microscopy, Elisa Dultz, Carmen Weber, Stephanie Heinrich, Mostafa Zedan, Sarah Khawaja
541 Evgeny Onishchenko, and Jan Nagler for their critical reading of this manuscript and members of the
542 Weis lab for helpful discussions and comments. We would also like to thank Bram Hofland for assisting
543 in cloning of yeast constructs. M.H. was supported by a Human Frontier Science Program (HFSP)
544 postdoctoral fellowship (LT000914/2015) and an ETH postdoctoral fellowship (FEL-37-14-2). This work

545 was supported by NIH/NIGMS (R01GM058065 and R01GM101257 to K.W.) and the Swiss National
546 Science Foundation (SNF 31003A_159731 and 31003A_179275 to K.W.).

547

548 **Figure legends**

549 **Figure 1. (A) Overexpression (OE) of Pat1 leads to constitutive PB formation but only in the presence**
550 **of Dhh1.** Cells co-expressing the indicated PB components were grown in synthetic complete (SC)
551 raffinose media to exponential growth phase after which Pat1 was overexpressed via addition of
552 galactose. Cells in both raffinose and galactose were observed by fluorescence microscopy. In all Pat1
553 OE strains the endogenous promoter of Pat1 was replaced by the galactose 1-10 promoter (*p-GAL-*
554 *PAT1*). Scale bar: 5µm. (B) Quantification of images in A depicting number of PBs/cell. N= 3 biological
555 replicates with >800 cells/replicate. Error bars: SEM. (C) **Pat1-NC (AA 5-79 + 456-587) is functional *in***
556 ***vivo*.** Cartoon of the Pat1-NC construct (see text for details). **(D) *PAT1-NC* induces PB formation upon**
557 **stress *in vivo***. Cells co-expressing the indicated the PB components in *PAT1* full length or *PAT1-NC*
558 background were grown in synthetic complete (SCD) media to exponential growth phase then shifted
559 to glucose-rich or glucose-starvation conditions for 30 minutes and observed by fluorescence
560 microscopy. PBs induced in the *PAT1-NC* background were dissolved by addition of 2% glucose
561 demonstrating reversibility. Scale bar: 5µm. (E) Quantification of images shown in A depicting number
562 of PBs/cell. Bars: SEM. N=3 biological replicates with >800 cells/replicate. **(F) *PAT1-NC* (AA 5-79 + 456-**
563 **587) OE leads to constitutive PB induction**. *p(GAL)-PAT1* or *p(GAL)-PAT1-NC* cells expressing Dhh1-
564 GFP were grown in SC raffinose media to exponential growth phase after which Pat1 OE was induced
565 with galactose. Scale bar: 5µm. (G) Graph depicts Dhh1 PBs/cell, SEM. N= 3 biological replicates with
566 >800 cells/replicate. [Diatrack 3.05 and cell segmentation using in house Matlab code was used for the
567 quantification of PB and cell numbers respectively for all the experiments shown in the manuscript].

568 **Figure Supplementary S1. (A) Controls for the Pat1 OE, relating to Figure 1.** Upper panel: *PAT1*
569 (endogenous promoter) cells expressing Dhh1-GFP were grown in (SC) raffinose media to exponential

570 growth phase after which galactose was added and cells were imaged by fluorescence microscopy.
571 Lower Panel: *p(GAL)-HA pat1Δ* (Hemagglutinin tag) OE does not lead to constitutive PB formation.
572 Scale bar: 5µm. **(B) *PAT1-NC* rescues the *pat1Δ* growth phenotype**. *PAT1, pat1Δ* and *PAT1-NC* cells
573 were grown overnight in SCD media to saturation and the next day the different strains were
574 inoculated to OD 0.1 in SCD. Absorbance based growth measurements were recorded for 24 hours.
575 The growth curve depicts O.D. 600 nm versus time. **(C) Pat1-NC localizes to PBs upon stress *in vivo*.**
576 Cells co-expressing Pat1-NC-GFP and Dcp2-mCherry as an additional PB marker were grown in SCD
577 media to exponential growth phase then shifted to glucose-rich or glucose-starvation conditions for
578 30 minutes and observed by fluorescence microscopy. After visualization 2% final concentration of
579 glucose was added for one hour to demonstrate reversibility and dissolution of Pat1-NC PBs. Scale bar:
580 5µm.

581 **Figure 2. (A) Recombinant Pat1-NC$^{4A\text{-}Dhh1}$ is defective for Dhh1 binding.** GST pull-down with GST-Pat1-
582 NC and mutants thereof as matrix-bound bait and Dhh1 as prey. After 1h of binding at 4°C, the samples
583 were washed 5 times with a buffer containing 300 mM NaCl and visualized by Coomassie staining after
584 separation on a 12 % acrylamide gel. **(B) Expression of *pat1* $^{4A\text{-}Dhh1}$ (Dhh1 binding mutant) leads to a**
585 **drastic reduction in PB formation.** Cells co-expressing the indicated PB components in the *PAT1* or
586 *pat1*$^{4A\text{-}Dhh1}$ background were grown in SCD media to exponential growth phase, then shifted to glucose-
587 rich or glucose-starvation conditions for 30 minutes and observed by fluorescence microscopy. Scale
588 bar: 5µm. (C) Quantification of images in B depicting number of PBs/cell, (Dhh1-GFP PBs co-localizing
589 with Dcp2-mCherry) are shown, bars: SEM. (D) ***Pat1*** $^{4A\text{-}Dhh1}$ **mutant is defective for PB localization.** Cells
590 expressing either Pat1-GFP or the Pat1$^{4A\text{-}Dhh1}$-GFP mutant were grown in SCD media to exponential
591 growth phase then shifted to glucose-rich or glucose-starvation conditions for 30 minutes and
592 observed by fluorescence microscopy. Scale bar: 5µm. (E) Quantification of images shown in D
593 depicting number of PBs/cell. N= 3 biological replicates with >500 cells/replicate. Error bars: SEM. (F)
594 ***pat1*$^{4A\text{-}Dhh1}$ mutant is defective in PB formation upon hippuristanol treatment.** Cells expressing either
595 *PAT1* or the *pat1*$^{4A\text{-}Dhh1}$ were grown in SCD media to exponential growth phase after which they were

596 treated with 10uM hippuristanol for 2hrs. The kinetics of PB formation was monitored using Dhh1-GFP
597 and its co-localization with Dcp2-mCherry. Quantification of PBs/cell is depicted. Stills from the live
598 imaging time course are shown. N= 2 biological replicates with >300 cells/replicate, SD.

599 **Figure Supplementary S2. (A) *pat1$^{4A\text{-}Dhh1}$* mutant has a slight growth defect.** *PAT1*, *pat1Δ* and *pat1$^{4A\text{-}}$*
600 *^{Dhh1}* cells were grown overnight in SCD media to saturation and the next day the different strains were
601 inoculated to OD 0.1 and growth curves were recorded for 24 hours. The growth curve depicts O.D.
602 600 nm versus time. **(B) *pat1Δ* abolishes PB formation.** Cells expressing Dhh1-GFP in *pat1Δ or PAT1*
603 strains were grown in SCD media to exponential growth phase then shifted to glucose-rich or glucose-
604 starvation conditions for 30 minutes and observed by fluorescence microscopy. The graph depicts the
605 number of PBs/cell. N=2 biological replicates, 300 cells per replicate, SD.

606 **Figure 3. (A, B) Overexpression (OE) of *p(GAL)-PAT1^{WT}*(wild type) and *p(GAL)-pat1^{AA}* (non-**
607 **phosphorylatable) leads to constitutive PB formation but OE of *p(GAL)-pat1^{EE}* (phospho-mimic) does**
608 **not.** Cells co-expressing the indicated PB components were grown in SC raffinose media to exponential
609 growth phase after which OE of different Pat1 alleles was induced by galactose addition. Cells were
610 imaged using fluorescence microscopy. Quantification of images shown in C depicting number of
611 PBs/cell. Scale bar: 5µm, SEM. N=3 biological replicates with >800 cells/replicate. (C) **Pat1-C-terminal**
612 **domain does not bind Dhh1.** V5 pull-down with V5-Pat1-C and V5-Pat1-C^{EE} as matrix-bound bait and
613 Dhh1-mCherry as prey. After 1h of binding at 4°C, the samples were washed 4 times with a buffer
614 containing NaCl as indicated and visualized by Coomassie staining after separation on a 12 %
615 acrylamide gel. **(D) Pat1-C^{EE} weakens the interaction with RNA compared to Pat1-C.** Recombinant
616 Pat1-C (WT) and Pat1-C^{EE} were incubated with a Cy5-labeld 29nt RNA oligo in the presence of 300mM
617 NaCl and separated on a NativePage gradient gel. The fluorescence of the oligo was detected by LI-
618 COR imaging. Reactions were performed in triplicate and the intensity of the upper shifted RNA oligo
619 band was quantified. Equal input of the Pat1-C proteins was verified by acrylamide PAGE and
620 Coomassie staining. Error bars: SD.

621 **Figure Supplementary S3. *PAT1* and *pat1* ^{AA} lead to PB induction upon stress, which is drastically**
622 **reduced in the *pat1*^{EE} background.** (A) Cells expressing the indicated GFP-PB markers (in the *PAT1*$^{WT/SS}$,
623 *pat1*^{AA} and *pat1*^{EE} backgrounds) were grown in SCD media to exponential growth phase then shifted to
624 glucose-rich (left panel) or glucose-starvation conditions (right panel) for 30 minutes and observed by
625 fluorescence microscopy. Scale bar: 5µm. (B) Quantification of images shown in A depicting PBs/cell.
626 Bars:SEM, N= 3 biological replicates with >800 cells/replicate.

627 **Figure 4. (A) *not1*$^{9X\text{-}Dhh1}$ (Dhh1 binding mutant) combined with *pat1*^{AA} (non-phosphorylatable Pat1)**
628 **enhances constitutive PB formation.** Cells expressing either *not1*$^{9X\text{-}Dhh1}$ or *pat1*^{AA} or the combination
629 of both mutants were grown in SCD media to exponential growth phase and PBs visualized by
630 fluorescence microscopy using Dcp2-mCherry as a *bona fide* PB marker. Scale bar: 5µm. (B) The graph
631 depicts the number of Dcp2 positive PBs/cell. N= 2 biological replicates with >500 cells visualized in
632 each replicate, bars: SEM.

633 **Figure Supplementary S4. (A) Pat1 does not inhibit the Not1^{MIF4G}-stimulatd ATPase activity of Dhh1**.
634 ATPase reactions were performed under saturating concentrations of polyU using a Not1^{MIF4G}
635 concentration that stimulates Dhh1 to 0.75 V_{max}. Pat1 was added to either 2- and 6-fold excess over
636 Not1. Three biological replicates (each of three technical replicates); mean and standard deviation of
637 k_{cat} values. The values are corrected for blank (that is Pat1 alone or Not1 alone). P values are obtained
638 from a two-tailed t-test. **(B) Pat1 OE PBs are more dynamic than the Dhh1^{DQAD} PBs.** Cells expressing
639 Dcp2-mCherry in the *p(GAL)-PAT1* OE strain were grown in (SC) raffinose to exponential growth phase
640 after which galactose was added to 2% final concentration for 2hrs to induce PBs. Then the cells were
641 treated with 50µg/ml cycloheximide (CHX) and disappearance of Dcp2-mCherry PBs per cell was
642 monitored for 90 minutes by fluorescence microscopy. In order to study PB dynamics in the *DHH1* and
643 *dhh1* ^{DQAD} background cells were grown as described before except PBs were induced by carbon
644 starvation and their disassembly monitored by CHX. Each time point shows a representative image. (B)
645 The graph shows the foci number per cell measurements for Dcp2-mCherry normalized to 1 to account

646 for differences in PB formation under different PB induction conditions. Scale bar: 5µm. N=2 biological
647 replicates with >200 cells counted per experiments. Error bars: SD.

648 **Figure 5. Pat1 WT but not Pat1$^{4A\text{-}Dhh1/EE}$ mutant enhances the phase separation of Dhh1 and RNA *in*
649 *vitro*.** (A) 4 µM Dhh1-mCherry was mixed with 3.2 mM ATP and 0.2 mg/ml polyU as RNA-analog in a
650 150mM KCl buffer. Pat1-NC-GFP and mutants thereof were added in increasing concentrations, as
651 indicated. mCherry and GFP intensities are scaled identically in all images displayed. Representative
652 images, scale bar 25 µm. Quantification of the droplet intensity multiplied by area (mCherry and GFP
653 channels separately normalized to Dhh1 alone and Pat1 4µM respectively) of three technical replicates
654 of the reactions displayed in Figure 5A, mean and standard deviation. (B) **Not1 prevents droplet
655 formation also in the presence of Pat1**. Proteins were mixed as indicated, and droplet formation
656 induced by addition of low salt buffer, ATP and polyU. Scale bar 25 mM, quantification (intensity
657 multiplied by area) of two biological replicates (one to three technical replicates each), mean and
658 standard deviation.

659 **Figure Supplementary S5.** (A) **Pat1 by itself does not phase separate *in vitro*.** Reactions are performed
660 in the presence of ATP and polyU at indicated protein concentrations.

661 **Figure 6. Stoichiometry of Pat1 and Dhh1 in PBs *in vivo* and in liquid droplets *in vitro*.** (A) Pat1-GFP
662 and Dhh1-GFP expressing cells were grown in SCD media to exponential growth phase and then shifted
663 to SC (minus glucose) for the indicated time points. PB formation was visualized by fluorescence
664 microscopy. Graph depicts the ratio of Dhh1: Pat1 in PBs *in vivo*. (B) Calibration curves to determine
665 the protein concentration of Dhh1-mCherry and Pat1-NC-GFP within the droplets: the fluorescence
666 intensity of homogeneous solutions of the respective proteins was measured at different protein
667 concentrations (blue circles). The unknown protein concentration was determined by linear fitting of
668 this calibration curve (violet circle). Confocal fluorescence microscopy images of phase-separated
669 droplets of Dhh1-mCherry in the absence and presence of Pat1-GFP are shown. Scale bar: 20µM. **(C)
670 Tug-of-war model between Pat1 and Not1 to regulate PB dynamics.** Model depicting three inputs

671 that cooperatively regulate PB formation. The solid black arrows on the left show interaction between
672 the Pat1 N-terminus with the RecA2 core of Dhh1, Pat1 C-terminus with RNA, Dhh1 interaction with
673 RNA and potential Dhh1-Dhh1 interactions via low-complexity unstructured tails. The dotted grey
674 arrows on the right demonstrate multivalent interactions in a PB driven by the LLPS of Dhh1 and RNA
675 (a process enhanced by Pat1). Colors: green: inputs that promote PB assembly, red factors that
676 negatively regulate PB formation. Violet: Dhh1, light green: Pat1-NC, blue: RNA.

677 **Figure Supplementary S6. (A) Images of the Pat1-GFP and Dhh1-GFP stoichiometry**. Cells expressing
678 Pat1-GFP and Dhh1-GFP were grown in SCD media to exponential growth phase then shifted to
679 glucose-starvation conditions for different time points as indicated and PBs were imaged by
680 fluorescence microscopy. Images are representative for each times. Scale: 5µM. (B) Dhh1-GFP and
681 Pat1-GFP expressing cells (used for imaging in A) were grown in SCD media to exponential growth
682 phase and protein levels were measured using Western blot with an anti-GFP antibody. Hexokinase
683 was used as a loading control. The graph depicts the expression levels of Dhh1 and Pat1 normalized to
684 the loading control. (C) **Size distributions of *in vitro* assembled Dhh1 and Pat1 LLPS droplets** (relating
685 to Figure 6B). In presence of Pat1, the droplet size increases and the size distribution shifts to larger
686 radii. Moreover, the number of droplets decreases, thereby indicating that the droplets have higher
687 propensity to fuse in presence of Pat1. Scale bar: 20µm.

688 **Figure Supplementary S7. OE of Pat1 on top of the endogenous copy of Pat1 [*p-PAT1* +p(GAL)-*PAT1*]**
689 **leads to the nuclear localization of PB components.** Cells expressing Dhh1-GFP [*p-PAT1* +p(GAL)-*PAT1*
690 background] were grown in SC raffinose media to exponential growth phase after which Pat1 OE was
691 induced with galactose. Localization of Dhh1-GFP to the nucleus was confirmed by co-localization with
692 DAPI staining after 2hrs of *PAT1* or $pat1^{AA}$ OE. White arrows depict the co-localization of Dhh1-GFP and
693 DAPI. Scale bar: 5µm. N= 2 biological replicates. (B) HDEL Td tomato was used as a marker of the
694 nuclear rim, scale bar: 5µm. **(C) PBs formed in $pat1^{4A\text{-}Dhh1}$ and $pat1^{EE}$ expressing cells are less intense**

695 **than PBs formed in *PAT1* wild-type cells.** Graph showing the average intensity of PBs (obtained from
696 Figure 2B and S3).

697 **Movie legends**

698 Movie 1: **Hippuristanol induces PBs in cells expressing wild-type *PAT1***. The movie depicts PB
699 formation (Dhh1-GFP and Dcp2-mCherry co-localization) in cells expressing wild-type *PAT1* upon
700 hippuristanol treatment. (2hrs movie, 5 min intervals; movie played at 7 fps). Each frame is a single
701 plane.

702 Movie 2: **Hippuristanol fails to induce PBs in cells expressing *pat1*$^{4A\text{-}Dhh1}$ mutant.** The movie depicts
703 failure to form PBs (Dhh1-GFP and Dcp2-mCherry co-localization) in cells expressing *pat1*$^{4A\text{-}Dhh1}$ upon
704 hippuristanol treatment. (2hrs movie, 5 min intervals; movie played at 7 fps). Each frame is a single
705 plane.

706 Movie 3: **Cycloheximide treatment causes wild-type PB disassembly.** Dcp2-mCherry expressing cells
707 in the *DHH1* background were grown in (SC) raffinose media to exponential growth phase, after which
708 galactose was added to 2% final concentration for 2hrs and then starved for 30 mins to allow PBs to
709 form. The cells were then treated with 50 µg/mL cycloheximide for 90 mins and disappearance of foci
710 was monitored using fluorescence microscopy. (5 min intervals; movie played at 7 fps). Each frame is
711 a single plane.

712 Movie 4: **Cycloheximide treatment causes Pat1 OE PB disassembly albeit faster than PB disassembly**
713 **in cells expressing *dhh1* ^{DQAD}.** Cells expressing Dcp2-mCherry in the *p(GAL)-PAT1* OE strain were grown
714 in (SC) raffinose to exponential growth phase, after which galactose was added to 2% final
715 concentration for 2hrs to allow PBs to form. Thereafter, the cells were treated with 50µg/mL
716 cycloheximide (CHX) for 90 mins and disappearance of foci was monitored using fluorescence
717 microscopy. (5 min intervals; movie played at 7 fps). Each frame is a single plane.

718 Movie 5: **Cycloheximide treatment of *dhh1* ^{DQAD} PBs.** Dcp2-mCherry expressing cells in the *dhh1*^{DQAD}
719 mutant background were grown in (SC) raffinose to exponential growth phase, after which galactose

720 was added to 2% final concentration for 2hrs. The cells were then carbon starved for 30 mins to allow
721 PBs to form after which, 50 µg/mL cycloheximide was added and disappearance of foci was monitored
722 for 90 mins using fluorescence microscopy. (5 min intervals; movie played at 7 fps). Each frame is a
723 single plane.

724 **SUPPLEMENTARY TABLE S1**

725 **Yeast strains in this study**

Strain #	**Genotype**
KWY165	*MAT a ade2-1 can1-100 GAL phi+ his3-11,15 ura3-1 leu2-3, 112 trp1-1*
KWY276	*MAT a ade2-1 can1-100 GAL phi+ his3-11,15 ura3-1 leu2-3, 112 trp1-1 dhh1::DHH1-GFP-HisMX6*
KWY1972	*MAT a ade2-1 can1-100 GAL phi+ his3-11,15 ura3-1 leu2-3, 112 trp1-1 dcp2::DCP2-mCherry-NatMX6*
KWY1973	*MAT a ade2-1 can1-100 GAL phi+ his3-11,15 ura3-1 leu2-3, 112 trp1-1 dhh1::DHH1-HisMX6 GFP dcp2::DCP2-mCherry-NatMX6*
KWY2226	*MAT a ade2-1 can1-100 GAL phi+ his3-11,15 ura3-1 leu2-3, 112 trp1-1 pat1Δ::KanMX6*
KWY3238	*MAT alpha ade2-1 can1-100 GAL phi+ his3-11,15 ura3-1 leu2-3, 112 trp1-1 dhh1Δ::KanMX6 dcp2::DCP2-mCherry-NatMX6 pDHH1-GFP-URA3*
KWY3239	*MAT alpha ade2-1 can1-100 GAL phi+ his3-11,15 ura3-1 leu2-3, 112 trp1-1 dhh1Δ::KanMX6 dcp2::DCP2-mCherry-NatMX6 pDHH1^{DQAD}-GFP-URA3*

KWY3280	*MAT a ade2-1 can1-100 GAL phi+ his3-11,15 ura3-1 leu2-3, 112 trp1-1 pat1::PAT1-GFP-HisMX6*
KWY4901	*MAT alpha ade2-1 can1-100 GAL phi+ his3-11,15 ura3-1 leu2-3, 112 trp1-1 dhh1Δ::KanMX6 dcp2::DCP2-mCherry-NatMX6 pDHH1$^{5X\text{-}Not}$-GFP-URA3*
KWY5157	*MAT alpha ade2-1 can1-100 GAL phi+ his3-11,15 ura3-1 leu2-3, 112 trp1-1 dhh1Δ::TRP dhh1Δ::KanMX6*
KWY5221	*MAT alpha ade2-1 can1-100 GAL phi+ his3-11,15 ura3-1 leu2-3, 112 trp1-1 dhh1Δ::TRP pat1Δ::KanMX6 pDHH1 GFP-URA3*
KWY5224	*MAT alpha ade2-1 can1-100 GAL phi+ his3-11,15 ura3-1 leu2-3, 112 trp1-1 dhh1Δ::TRP pat1Δ::KanMX6 pDHH1^{DQAD}-GFP-URA3*
KWY5227	*MAT alpha ade2-1 can1-100 GAL phi+ his3-11,15 ura3-1 leu2-3, 112 trp1-1 dhh1Δ::TRP pat1Δ::KanMX6 pDHH1^{RNA3X}-GFP-URA3*
KWY5230	*MAT alpha ade2-1 can1-100 GAL phi+ his3-11,15 ura3-1 leu2-3, 112 trp1-1 dhh1Δ::TRP pat1Δ::KanMX6 pDHH1$^{DQAD/RNA3X}$-GFP-URA3*
KWY5601	*MAT a ade2-1 can1-100 GAL phi+ his3-11,15 ura3-1 leu2-3, 112 trp1-1 pat1:: PAT1-HisMX6 dhh1::DHH1 GFP-URA3*
KWY5603	*MAT a ade2-1 can1-100 GAL phi+ his3-11,15 ura3-1 leu2-3, 112 trp1-1 pat1::PAT1 AA::HisMX6 dhh1::DHH1 GFP-URA3*
KWY5609	*MAT a ade2-1 can1-100 GAL phi+ his3-11,15 ura3-1 leu2-3, 112 trp1-1 pat1::PAT1 EE-HisMX6 dhh1::DHH1 GFP-URA3*

KWY5915	*MAT alpha ade2-1 can1-100 GAL phi+ his3-11,15 ura3-1 leu2-3, 112 trp1-1 dhh1Δ::TRP pat1Δ::KanMX6 edc3::EDC3-mcherry:: HisMX6 pDHH1 GFP-URA3*
KWY5917	*MAT alpha ade2-1 can1-100 GAL phi+ his3-11,15 ura3-1 leu2-3, 112 trp1-1 dhh1Δ::TRP pat1Δ::KanMX6 edc3::EDC3-mcherry:: HisMX6 pDHH1^{DQAD}-GFP-URA3*
KWY5933	*MAT alpha ade2-1 can1-100 GAL phi+ his3-11,15 ura3-1 leu2-3, 112 trp1-1 dhh1Δ::TRP pat1Δ::KanMX6 dcp2::DCP2-mcherry:: HisMX6 pDHH1 GFP-URA3*
KWY5935	*MAT alpha ade2-1 can1-100 GAL phi+ his3-11,15 ura3-1 leu2-3, 112 trp1-1 dhh1Δ::TRP pat1Δ::KanMX6 dcp2::DCP2-mcherry:: HisMX6 pDHH1^{DQAD}-GFP-URA3*
KWY5943	*MAT alpha ade2-1 can1-100 GAL phi+ his3-11,15 ura3-1 leu2-3, 112 trp1-1 pat1:: PAT14A-HisMX6*
KWY5978	*MAT alpha ade2-1 can1-100 GAL phi+ his3-11,15 ura3-1 leu2-3, 112 trp1-1 pat1:: PAT1-HisMX6 dhh1::DHH1 GFP-URA3 pGAL-PAT1-3XV5-LEU2*
KWY5980	*MAT alpha ade2-1 can1-100 GAL phi+ his3-11,15 ura3-1 leu2-3, 112 trp1-1 pat1:: PAT1-HisMX6 dhh1::DHH1 GFP-URA3 pGAL-PAT1AA-3XV5-LEU2*
KWY5983	*MAT alpha ade2-1 can1-100 GAL phi+ his3-11,15 ura3-1 leu2-3, 112 trp1-1 pat1:: PAT1-HisMX6 dhh1::DHH1 GFP-URA3 pGAL-PAT1 EE-3XV5-LEU2*
KWY6003	*MAT alpha ade2-1 can1-100 GAL phi+ his3-11,15 ura3-1 leu2-3, 112 trp1-1 pat1Δ::KanMX6 dhh1Δ::TRP pDHH1$^{5X\text{-}Not}$-GFP-URA3*

KWY6056	*MAT alpha ade2-1 can1-100 GAL phi+ his3-11,15 ura3-1 leu2-3, 112 trp1-1 pat1::PAT14A-HismX6 dhh1Δ::TRP pDHH1^{DQAD}-GFP-URA3*
KWY6058	*MAT alpha ade2-1 can1-100 GAL phi+ his3-11,15 ura3-1 leu2-3, 112 trp1-1 pat1::PAT14A-HismX6 dhh1Δ::TRP pDHH1-GFP-URA3*
KWY6180	*MAT alpha ade2-1 can1-100 GAL phi+ his3-11,15 ura3-1 leu2-3, 112 trp1-1 pGAL-PAT1 3X HA::KanMX6 dhh1::DHH1 GFP::URA3*
KWY6279	*MAT a ade2-1 can1-100 GAL phi+ his3-11,15 ura3-1 leu2-3, 112 trp1-1 pat1::PAT1-HisMX6 edc3::EDC3 GFP-URA3*
KWY6403	*MAT alpha ade2-1 can1-100 GAL phi+ his3-11,15 ura3-1 leu2-3, 112 trp1-1 pat1Δ::pGAL-3X HA::KanMX6 dhh1::DHH1 GFP URA3*
KWY6467	*MAT a ade2-1 can1-100 GAL phi+ his3-11,15 ura3-1 leu2-3, 112 trp1-1 pat1::PAT1AA-HisMX6 edc3::EDC3 GFP-URA3*
KWY6469	*MAT a ade2-1 can1-100 GAL phi+ his3-11,15 ura3-1 leu2-3, 112 trp1-1 pat1::PAT1AA-HisMX6 dcp2::DCP2 GFP-URA3*
KWY6471	*MAT a ade2-1 can1-100 GAL phi+ his3-11,15 ura3-1 leu2-3, 112 trp1-1 pat1::PAT1-HisMX6 dcp2::DCp2 GFP-URA3*
KWY6478	*MAT a ade2-1 can1-100 GAL phi+ his3-11,15 ura3-1 leu2-3, 112 trp1-1 pat1::PAT1EE-HisMX6 dcp2::DCP2 GFP-URA3*
KWY6480	*MAT a ade2-1 can1-100 GAL phi+ his3-11,15 ura3-1 leu2-3, 112 trp1-1 pat1::PAT1EE-HisMX6 edc3::EDC3 GFP-URA3*

KWY6544	*MAT a ade2-1 can1-100 GAL phi+ his3-11,15 ura3-1 trp1-1 leu2-3, 112Δ::CG-LEU2-NOT1$^{9X\text{-}Dhh1}$-TAP not1Δ::TRP1 dcp2::DCP2-mCherry-NatMX6*
KWY6637	*MAT alpha ade2-1 can1-100 GAL phi+ his3-11,15 ura3-1 leu2-3, 112 trp1-1 dhh1::DHH1 GFP-URA3 dcp2::DCP2-mCherry-NatMX6 pGAL-PAT1 AA-3XV5-LEU2*
KWY6643	*MAT alpha ade2-1 can1-100 GAL phi+ his3-11,15 ura3-1 leu2-3, 112 trp1-1 pGAL-PAT1-3X HA::KanmX6 dhh1::DHH1 GFP: URA3 dcp2::DCP2-mCherry-NatMX6*
KWY6692	*MAT alpha ade2-1 can1-100 GAL phi+ his3-11,15 ura3-1 leu2-3, 112 trp1-1 pGAL-PAT1 EE-3X-HA::KanMX6 dhh1::DHH1 GFP::URA3 dcp2::DCP2-mCherry-NatMX6*
KWY6836	*MAT alpha ade2-1 can1-100 GAL phi+ his3-11,15 ura3-1 leu2-3, 112 trp1-1 pGAL-PAT1 3XHA::URA3 dhh1Δ::KanMX6 edc3::EDC3 GFP-HisMX6 dcp2::DCP2-mCherry-NatMX6*
KWY7370	*MAT a ade2-1 can1-100 GAL phi+ his3-11,15 ura3-1 leu2-3, 112 trp1-1 pat1::p-GAL- PAT1 NC-3X-HA-HYG dhh1::DHH1 GFP-URA3*
KWY7420	*MAT alpha ade2-1 can1-100 GAL phi+ his3-11,15 ura3-1 leu2-3, 112 trp1-1 pGAL-PAT1 3XHA::KanMX6 dhh1::DHH1 RNA3X GFP-HismX6*
KWY7481	*MAT a ade2-1 can1-100 GAL phi+ his3-11,15 ura3-1 leu2-3, 112 trp1-1 pat1::PAT14A GFP-URA3*
KWY7484	*MAT a ade2-1 can1-100 GAL phi+ his3-11,15 ura3-1 leu2-3, 112 trp1-1 pat1::PAT1 NC-HYG dhh1::DHH1 GFP-HisMX6 dcp2::DCP2-mCherry-NatMX6*

KWY7554	*MAT a ade2-1 can1-100 GAL phi+ his3-11,15 ura3-1 leu2-3, 112 trp1-1 pat1::PAT14A GFP-URA3 dcp2::DCP2 mcherry-KanMX6*
KWY7557	*MAT a ade2-1 can1-100 GAL phi+ his3-11,15 ura3-1 leu2-3, 112 trp1-1 pat1::PAT1N-C GFP-HismX6*
KWY7562	*MAT a ade2-1 can1-100 GAL phi+ his3-11,15 ura3-1 leu2-3, 112 trp1-1 pat1::PAT1N-C GFP-HisMX6 dcp2::DCP2 mcherry-NatMX6*
KWY7890	*MAT a ade2-1 can1-100 GAL phi+ his3-11,15 ura3-1 leu2-3, 112 trp1-1 dhh1::dhh1^{DQAD}-GFP-HisMX6 dcp2::DCP2-mCherry-NatMX6*
KWY8378	*MAT a ade2-1 can1-100 GAL phi+ his3-11,15 ura3-1 trp1-1 leu2-3, 112Δ::CG-LEU2-NOT1$^{9X\text{-}Dhh1}$-TAP not1Δ::TRP1 pat1::PAT1AA-HisMX6 dcp2::DCP2-mCherry-NatMX6*

726

727 <u>SUPPLEMENTARY TABLE S2</u>

728 A) Plasmids used in this study

Plasmid #	Description
pKW2312	pRS316 P(DHH1)-DHH1-GFP
pKW2313	pRS316 P(DHH1)-DHH1^{DQAD}-GFP
pKW2867	pRS316 P(DHH1)-DHH1$^{3X\text{-}RNA}$-GFP
pKW3040	pRS316 P(DHH1)-DHH1$^{DQAD/3X\text{-}RNA}$-GFP
pKW3333	pRS316 P(DHH1)-DHH1$^{5X\text{-}Not}$-GFP

pKW3477	pRS316 P(DHH1)-DHH1$^{DQAD/3X-RNA}$-6xHis-PP7CP
pKW3756	pNH605-PGAL-Pat1 WT (XbaI)-3X V5
pKW3757	pNH605-PGAL- Pat1^{AA} (XbaI)-3X V5
pKW3758	pNH605-PGAL- Pat1^{EE} (XbaI)-3X V5
pKW3631	pETMCN_HisV5_Dhh1-mCherry
pKW3688	pETMCN_His_Dhh1-mCherry
pKW3641	pETMCN_HisV5_Pat1-C
pKW3702	pETMCN_HisV5_ Pat1-C^{EE}
pKW4225	pETMCN_GST-Pat1-NC-mCherry
pKW4356	pETMCN_GST-Pat1-NC-GFP
pKW4357	pETMCN_GST- Pat1-NC$^{4A-Dhh1}$-GFP
pKW4358	pETMCN_GST- Pat1-NC^{EE}-GFP

729

730

731 B) Dhh1, Pat1 and Not1 mutants used in this study

Mutant Protein	Mutation(s)
Dhh1^{DQAD}	E195Q
Dhh1$^{Q-motif}$	F66R, Q73A
Dhh1^{3X-RNA}	R322A, S340A, R370A
Dhh1^{5X-Not}	R55E, F62E, Q282E, N284E, R335E
Dhh1$^{DQAD/3X-RNA}$	E195Q, R322A, S340A, R370A
Dhh1$^{5X-Not/3X-RNA}$	R55E, F62E, Q282E, N284E, R322A, R335E, S340A, R370A

Not1$^{9X\text{-}Dhh1}$	F791A, N795A, K804A, E823R, N834A, Y835A, K962A, F967A, E970A
Pat1^{AA}	S456A S457A
Pat1^{EE}	S456E S457E
Pat1$^{4A\text{-}Dhh1}$	D39A E40A T41A F42A
Pat1-N-C	Pat1 N (5-79)- (GGS)4- C- (456-787)

732

733

734 C) Oligos used in this study

Oligo #	**Sequence**	**Description**
CH393	tgttcattattcatcatggaccaagccgataaaatgttatct cgt	DHH1, fw; mutagenic primer E195Q for Dhh1^{DQAD} mutant
CH394	acgagataacattttatcggcttggtccatgatgaataatga aca	DHH1, rev; mutagenic primer E195Q for Dhh1^{DQAD} mutant
CH574	atggtttttcaaaaccggcttcttcaatacccattaacagct ctcttttcaaataaaaatc	DHH1, rev; mutagenic primer F62E for Dhh1$^{5X\text{-}Not}$ mutant
CH575	cttaaatacaaagggtaatacttttgaagatttttatttgaa agaagagctgttaatgggtattttt	DHH1, fw; mutagenic primer R55E for Dhh1$^{5X\text{-}Not}$ mutant
CH576	gatttttatttgaaaagagagctgttaatgggtattgaagaa gccggttttgaaaaaccat	DHH1, fw; mutagenic primer F62E for Dhh1$^{5X\text{-}Not}$ mutant
CH577	aaaaatacccattaacagctcttctttcaaataaaaatcttc aaaagtattacccttttgtatttaag	DHH1, rev; mutagenic primer R55E for Dhh1$^{5X\text{-}Not}$ mutant

CH578	cacggttagtagaattacaaaaaataatggcttgctcaattcaagcttagagaataaagtatttaaacaatgtagc	DHH1, rev; mutagenic primer Q282E and N284E for Dhh1$^{5X\text{-}Not}$ mutant
CH579	gctacattgtttaaatactttattctctaagcttgaaattgagcaagccattatttttgtaattctactaaccgtg	DHH1, fw; mutagenic primer Q282E and N284E for Dhh1$^{5X\text{-}Not}$ mutant
CH580	atcggagcagaccaatgtttcaaccttaccttgacgaaattcgtgg	DHH1, rev; mutagenic primer R335E for Dhh1$^{5X\text{-}Not}$ mutant
CH581	ccacgaatttcgtcaaggtaaggttgaaacattggtctgctccgat	DHH1, fw; mutagenic primer R335E for Dhh1$^{5X\text{-}Not}$ mutant
Ch849	atcaaattcccctcttctgatgcttaattgccccgattgcagcctgttattgatactatt	For stich PCRs to make Pat1 AA and EE, pringle fw
CH853	taaaaaataagggagaaaaaaaaatacatgcgtaagtacattaaaattacaggaaaaatc gaattcgagctcgtttaaac	For stich PCRs to make Pat1 AA and EE , pringle rev
CH854	attaccgttgttgaacgcgtaagcagctcttcttctttgcttaga	For stich PCRs to make Pat1 AA, rev
CH855	tctaagcaaagaagaagagctgcttacgcgttcaacaacggtaat	For stich PCRs to make Pat1 AA, fw
CH856	attaccgttgttgaacgcgtattcttctcttcttctttgcttaga	For stich PCRs to make Pat1 EE, rev
CH857	tct aag caa aga aga aga gaa gaa tac gcg ttc aac aac ggt aat	For stich PCRs to make Pat1 EE, fw

CH858	ttaattaacccggggatccg ttactttagttctgatatttcaccatcgcgatacaccaacccc ataac	For stich PCRs to make Pat1 EE, rev
CH944	aacttcttcaagtcctgcttgtcccaggagggttcaggga	For stich PCRs to make Pat1 4A GFP tagged, fw
CH945	aac ctg aac att atc acc agc agc agc agc gttcaaatagtcgttctc	For stich PCRs to make Pat1 4A GFP tagged, rev
CH946	gaacgactatttgaac gct gct gct gct ggtgataatgttcaggttgg	For stich PCRs to make Pat1 4A GFP tagged, fw
CH1035	tttcatggcgatgccacctggtcagtcacaaccccagtat cggatccccgggttaattaa	Dhh1, fw; C-terminal GFP tagging
CH1036	gcgtatctcaccacagtagttatttttcttagatattct gaattcgagctcgtttaaac	Dhh1 rev; C-terminal GFP tagging
CH1037	ttcagggtctaatgaattattaagcattttgcataggaag cggatccccgggttaattaa	Dcp2, fw; C-terminal mcherry tagging
CH1038	catttacagtgtgtctataaaacgtataacacttattcttga attcgagctcgtttaaac	Dcp2, rev; C-terminal mcherry tagging
CH1039	tgatcttttcgtcactgacgggtccctgctattagatttgcgg atccccgggttaattaa	Edc3, C- terminal mcherry, fw
CH1040	tatacgtatgtatccagtttaggctaaagtaattcttggtga attcgagctcgtttaaac	Edc3, C- terminal mcherry, rev
CH1116	gaggagaacgactatttgaac gct gct gct gct ggtgataatgttcaggtt	For stich PCRs to make Pat1 4A GFP tagged, fw (pringle)
CH1117	aacctgaacattatcacc agc agc agc agc gttcaaatagtcgttctcctc	For stich PCRs to make Pat1 4A GFP tagged, rev (pringle)

CH1550	ttccccattttatcaaaaatcatcctgccaccattttgtccaa ggatcgcactatcgccc gaattcgagctcgtttaaac	Pgal-Pat1 tagging: fw
CH1551	ttcaaagtccagaggaccatcccgcgcattaccgctattttc taacccaaagaaggacat gcactgagcagcgtaatctg	Pgal-Pat1 tagging: rev
CH1768	aaaataagggagaaaaaaaaatacatgcgtaagtacatt aaaattacaggaaaaatctta gcactgagcagcgtaatctg	K/O Pat1 in Pgal-3HA-Pat1 : rev
CH1879	aaggttttaaccggaagtaagagcagcaagaagcactagc agaacgcggccgccagctgaa	Pat1, fw; C-terminal GFP tagging
CH1878	tacatgcgtaagtacattaaaattacaggaaaaatcttatg aattcgagctcgtttaaac	Pat1, rev; C-terminal GFP tagging
UC1943	ctcttgcgttactatggtggtattattgatgctaatacgggcg cataggccactagtggatc	For pat1 delete, rev
UC1942	aaggttttaaccggaagtaagagcagcaagaagcactagc agaacgcggccgccagctgaa	For pat1 delete,fw
CH2394	ttccccattttatcaaaaatcatcctgccaccattttgtccaa ggatcgcactatcgccctcactatagggagaccggca	Pgal-Pat1 tagging: fw
CH2395	ttcaaagtccagaggaccatcccgcgcattaccgctattttc taacccaaagaaggacat cattttgagatccgggtttt	Pgal-Pat1 tagging: rev
CH2762	gggttagaaaatagcggtaatgcgcgggatggtcctctgg	For stich PCRs to make Pat1 NC, fw
CH2768	tcgcttatttagaagtggcgcgttacttaagctcgagcataa cgtttaggaa	For stich PCRs to make Pat1 NC, rev
CH2769	cgttatgctcgagcttaagtaacgcgccacttctaaataag cgaatttctta	For stich PCRs to make Pat1 NC, fw

CH2790	ttaaagccttcgagcgtcccaaaaccttctcaagcaaggtttt tcagtataat	For stich PCRs to make Pat1 NC, rev
CH2791	taaaaaataagggagaaaaaaaaatacatgcgtaagtac attaaaattacaggaaaaatcttaaagccttcgagcgtccc aa	For stich PCRs to make Pat1 NC, rev
CH2766	gacgtcccggactatgcaggatcctatccatatgacgttcc agattacgctgctcagtgcgggttagaaaatagcggtaa	For Pat1 NC HYG (pgal OE), fw
CH3005	gtacaccttgaaggaagcaaaggttttaaccggaagtaag agcagcaagaagcactagca gggttagaaaatagcggtaa	For stich PCRs to make Pat1 NC, fw
CH3054	gggttagaaaatagcggtaatgcgcgggatggtcctctgg	For stich PCRs to make Pat1 NC GFP tagged, fw
CH3060	catgttaattaacccggggatccgcttaagctcgagcataa cgtttaggaac	For stich PCRs to make Pat1 NC GFP tagged, rev
CH3061	gttcctaaacgttatgctcgagcttaagcggatccccgggtt aattaacatg	For stich PCRs to make Pat1 NC GFP tagged, fw
Ch3062	gaattcgagctcgtttaaactggatggcggcgttagtatcg aatcgacagca	For stich PCRs to make Pat1 NC GFP tagged, rev
CH3058	gtacaccttgaaggaagcaaaggttttaaccggaagtaag agcagcaagaagcactagcagggttagaaaatagcggta a	For stich PCRs to make Pat1 NC GFP tagged, fw (pringle)
CH3063	taaaaaataagggagaaaaaaaaatacatgcgtaagtac attaaaattacaggaaaaatcgaattcgagctcgtttaaac t	For stich PCRs to make Pat1 NC GFP tagged, rev (pringle)
US5021	ttcgtacattggtctgcgccgatttattgacccgt	DHH1, fw; mutagenic primer S340A for Dhh1$^{3X\text{-}RNA}$ mutant

US5022	acgggtcaataaatcggcgcagaccaatgtacgaa	DHH1, rev; mutagenic primer S340A for Dhh1$^{3X\text{-}RNA}$ mutant
US5023	ccaaaacggcagaaacatatttacatgctattggtagatccggtagg	DHH1, fw; mutagenic primer R370A for Dhh1$^{3X\text{-}RNA}$ mutant
US5024	cctaccggatctaccaatagcatgtaaatatgtttctgccgttttgg	DHH1, rev; mutagenic primer R370A for Dhh1$^{3X\text{-}RNA}$ mutant
UC6097	atcccaggcctaaaatacgacaagaaagaaaatagtagta*atgggttccatcaataataa*	DHH1; fw; For integrating *DHH1* mutants into *dhh1Δ* strains
UC6098	tatctcaccacagtagttatttttcttagatattct*ttaatactggggttgtgactgac*	DHH1; rv; For integrating *DHH1* mutants into *dhh1Δ* strains

References

Aguzzi, A., & Altmeyer, M. (2016). Phase Separation: Linking Cellular Compartmentalization to Disease. *Trends Cell Biol, 26*(7), 547-558. doi:10.1016/j.tcb.2016.03.004

Alberti, S., & Hyman, A. A. (2016). Are aberrant phase transitions a driver of cellular aging? *Bioessays, 38*(10), 959-968. doi:10.1002/bies.201600042

Ashe, M. P., De Long, S. K., & Sachs, A. B. (2000). Glucose depletion rapidly inhibits translation initiation in yeast. *Mol Biol Cell, 11*(3), 833-848. doi:10.1091/mbc.11.3.833

Barbee, S. A., Estes, P. S., Cziko, A. M., Hillebrand, J., Luedeman, R. A., Coller, J. M., . . . Ramaswami, M. (2006). Staufen- and FMRP-containing neuronal RNPs are structurally and functionally related to somatic P bodies. *Neuron, 52*(6), 997-1009. doi:10.1016/j.neuron.2006.10.028

Beelman, C. A., & Parker, R. (1994). Differential effects of translational inhibition in cis and in trans on the decay of the unstable yeast MFA2 mRNA. *J Biol Chem, 269*(13), 9687-9692.

748 Bhattacharyya, S. N., Habermacher, R., Martine, U., Closs, E. I., & Filipowicz, W. (2006). Relief of
749 microRNA-mediated translational repression in human cells subjected to stress. *Cell, 125*(6), 1111-
750 1124. doi:10.1016/j.cell.2006.04.031

751 Bordeleau, M. E., Mori, A., Oberer, M., Lindqvist, L., Chard, L. S., Higa, T., . . . Pelletier, J. (2006).
752 Functional characterization of IRESes by an inhibitor of the RNA helicase eIF4A. *Nat Chem Biol, 2*(4),
753 213-220. doi:10.1038/nchembio776

754 Braun, K. A., Vaga, S., Dombek, K. M., Fang, F., Palmisano, S., Aebersold, R., & Young, E. T. (2014).
755 Phosphoproteomic analysis identifies proteins involved in transcription-coupled mRNA decay as
756 targets of Snf1 signaling. *Sci Signal, 7*(333), ra64. doi:10.1126/scisignal.2005000

757 Carroll, J. S., Munchel, S. E., & Weis, K. (2011). The DExD/H box ATPase Dhh1 functions in translational
758 repression, mRNA decay, and processing body dynamics. *J Cell Biol, 194*(4), 527-537.
759 doi:10.1083/jcb.201007151

760 Chan, L. Y., Mugler, C. F., Heinrich, S., Vallotton, P., & Weis, K. (2018). Non-invasive measurement of
761 mRNA decay reveals translation initiation as the major determinant of mRNA stability. *Elife. In press.*

762 Chowdhury, A., Kalurupalle, S., & Tharun, S. (2014). Pat1 contributes to the RNA binding activity of the
763 Lsm1-7-Pat1 complex. *Rna, 20*(9), 1465-1475. doi:10.1261/rna.045252.114

764 Coller, J. M., Tucker, M., Sheth, U., Valencia-Sanchez, M. A., & Parker, R. (2001). The DEAD box helicase,
765 Dhh1p, functions in mRNA decapping and interacts with both the decapping and deadenylase
766 complexes. *Rna, 7*(12), 1717-1727.

767 Coller, J., & Parker, R. (2004). Eukaryotic mRNA decapping. *Annu Rev Biochem, 73*, 861-890.
768 doi:10.1146/annurev.biochem.73.011303.074032

769 Coller, J., & Parker, R. (2005). General translational repression by activators of mRNA decapping. *Cell,*
770 *122*(6), 875-886. doi:10.1016/j.cell.2005.07.012

Cougot, N., Bhattacharyya, S. N., Tapia-Arancibia, L., Bordonne, R., Filipowicz, W., Bertrand, E., & Rage, F. (2008). Dendrites of mammalian neurons contain specialized P-body-like structures that respond to neuronal activation. *J Neurosci, 28*(51), 13793-13804. doi:10.1523/jneurosci.4155-08.2008

Decker, C. J., Teixeira, D., & Parker, R. (2007). Edc3p and a glutamine/asparagine-rich domain of Lsm4p function in processing body assembly in Saccharomyces cerevisiae. *J Cell Biol, 179*(3), 437-449. doi:10.1083/jcb.200704147

Ernoult-Lange, M., Baconnais, S., Harper, M., Minshall, N., Souquere, S., Boudier, T., . . . Weil, D. (2012). Multiple binding of repressed mRNAs by the P-body protein Rck/p54. *Rna, 18*(9), 1702-1715. doi:10.1261/rna.034314.112

Fischer, N., & Weis, K. (2002). The DEAD box protein Dhh1 stimulates the decapping enzyme Dcp1. *Embo j, 21*(11), 2788-2797. doi:10.1093/emboj/21.11.2788

Franks, T. M., & Lykke-Andersen, J. (2008). The control of mRNA decapping and P-body formation. *Mol Cell, 32*(5), 605-615. doi:10.1016/j.molcel.2008.11.001

Fromm, S. A., Kamenz, J., Noldeke, E. R., Neu, A., Zocher, G., & Sprangers, R. (2014). In vitro reconstitution of a cellular phase-transition process that involves the mRNA decapping machinery. *Angew Chem Int Ed Engl, 53*(28), 7354-7359. doi:10.1002/anie.201402885

Fromm, S. A., Truffault, V., Kamenz, J., Braun, J. E., Hoffmann, N. A., Izaurralde, E., & Sprangers, R. (2012). The structural basis of Edc3- and Scd6-mediated activation of the Dcp1:Dcp2 mRNA decapping complex. *Embo j, 31*(2), 279-290. doi:10.1038/emboj.2011.408

Guo, L., & Shorter, J. (2015). It's Raining Liquids: RNA Tunes Viscoelasticity and Dynamics of Membraneless Organelles. *Mol Cell, 60*(2), 189-192. doi:10.1016/j.molcel.2015.10.006

Hadjidemetriou, S., Gabrielli, B., Pike, T., Stevens, F., Mele, K., & Vallotton, P. (2014). *Detection and Tracking of Cell Divisions in Phase Contrast Video Microscopy*. Paper presented at the Third MICCAI Worshop on Microscopic ImageAnalysis with Applications in Biology.

795 Holmes, L. E., Campbell, S. G., De Long, S. K., Sachs, A. B., & Ashe, M. P. (2004). Loss of translational
796 control in yeast compromised for the major mRNA decay pathway. *Mol Cell Biol, 24*(7), 2998-3010.

797 Hu, W., Sweet, T. J., Chamnongpol, S., Baker, K. E., & Coller, J. (2009). Co-translational mRNA decay in
798 Saccharomyces cerevisiae. *Nature, 461*(7261), 225-229. doi:10.1038/nature08265

799 Hyman, A. A., Weber, C. A., & Julicher, F. (2014). Liquid-liquid phase separation in biology. *Annu Rev*
800 *Cell Dev Biol, 30*, 39-58. doi:10.1146/annurev-cellbio-100913-013325

801 Kroschwald, S., Maharana, S., Mateju, D., Malinovska, L., Nuske, E., Poser, I., . . . Alberti, S. (2015).
802 Promiscuous interactions and protein disaggregases determine the material state of stress-inducible
803 RNP granules. *Elife, 4*, e06807. doi:10.7554/eLife.06807

804 Larimer, F. W., & Stevens, A. (1990). Disruption of the gene XRN1, coding for a 5'----3' exoribonuclease,
805 restricts yeast cell growth. *Gene, 95*(1), 85-90.

806 Longtine, M. S., McKenzie, A., 3rd, Demarini, D. J., Shah, N. G., Wach, A., Brachat, A., . . . Pringle, J. R.
807 (1998). Additional modules for versatile and economical PCR-based gene deletion and modification in
808 Saccharomyces cerevisiae. *Yeast, 14*(10), 953-961. doi:10.1002/(sici)1097-
809 0061(199807)14:10<953::Aid-yea293>3.0.Co;2-u

810 Lui, J., Castelli, L. M., Pizzinga, M., Simpson, C. E., Hoyle, N. P., Bailey, K. L., . . . Ashe, M. P. (2014).
811 Granules harboring translationally active mRNAs provide a platform for P-body formation following
812 stress. *Cell Rep, 9*(3), 944-954. doi:10.1016/j.celrep.2014.09.040

813 Mager, W. H., & Ferreira, P. M. (1993). Stress response of yeast. *Biochem J, 290 (Pt 1)*, 1-13.

814 Montpetit, B., Thomsen, N. D., Helmke, K. J., Seeliger, M. A., Berger, J. M., & Weis, K. (2011). A
815 conserved mechanism of DEAD-box ATPase activation by nucleoporins and InsP6 in mRNA export.
816 *Nature, 472*(7342), 238-242. doi:10.1038/nature09862

817 Mugler, C. F., Hondele, M., Heinrich, S., Sachdev, R., Vallotton, P., Koek, A. Y., . . . Weis, K. (2016).
818 ATPase activity of the DEAD-box protein Dhh1 controls processing body formation. *Elife, 5*.
819 doi:10.7554/eLife.18746

820 Muhlrad, D., & Parker, R. (1992). Mutations affecting stability and deadenylation of the yeast MFA2
821 transcript. *Genes Dev, 6*(11), 2100-2111.

822 Nissan, T., Rajyaguru, P., She, M., Song, H., & Parker, R. (2010). Decapping activators in Saccharomyces
823 cerevisiae act by multiple mechanisms. *Mol Cell, 39*(5), 773-783. doi:10.1016/j.molcel.2010.08.025

824 Ozgur, S., & Stoecklin, G. (2013). Role of Rck-Pat1b binding in assembly of processing-bodies. *RNA Biol,*
825 *10*(4), 528-539. doi:10.4161/rna.24086

826 Patel, A., Lee, H. O., Jawerth, L., Maharana, S., Jahnel, M., Hein, M. Y., . . . Alberti, S. (2015). A Liquid-
827 to-Solid Phase Transition of the ALS Protein FUS Accelerated by Disease Mutation. *Cell, 162*(5), 1066-
828 1077. doi:10.1016/j.cell.2015.07.047

829 Pilkington, G. R., & Parker, R. (2008). Pat1 contains distinct functional domains that promote P-body
830 assembly and activation of decapping. *Mol Cell Biol, 28*(4), 1298-1312. doi:10.1128/mcb.00936-07

831 Pillai, R. S. (2005). MicroRNA function: multiple mechanisms for a tiny RNA? *Rna, 11*(12), 1753-1761.
832 doi:10.1261/rna.2248605

833 Protter, D. S. W., Rao, B. S., Van Treeck, B., Lin, Y., Mizoue, L., Rosen, M. K., & Parker, R. (2018).
834 Intrinsically Disordered Regions Can Contribute Promiscuous Interactions to RNP Granule Assembly.
835 *Cell Rep, 22*(6), 1401-1412. doi:10.1016/j.celrep.2018.01.036

836 Radhakrishnan, A., Chen, Y. H., Martin, S., Alhusaini, N., Green, R., & Coller, J. (2016). The DEAD-Box
837 Protein Dhh1p Couples mRNA Decay and Translation by Monitoring Codon Optimality. *Cell, 167*(1),
838 122-132.e129. doi:10.1016/j.cell.2016.08.053

839 Ramachandran, V., Shah, K. H., & Herman, P. K. (2011). The cAMP-dependent protein kinase signaling
840 pathway is a key regulator of P body foci formation. *Mol Cell, 43*(6), 973-981.
841 doi:10.1016/j.molcel.2011.06.032

842 Ramaswami, M., Taylor, J. P., & Parker, R. (2013). Altered ribostasis: RNA-protein granules in
843 degenerative disorders. *Cell, 154*(4), 727-736. doi:10.1016/j.cell.2013.07.038

844 Rao, B. S., & Parker, R. (2017). Numerous interactions act redundantly to assemble a tunable size of P
845 bodies in Saccharomyces cerevisiae. *Proc Natl Acad Sci U S A, 114*(45), E9569-e9578.
846 doi:10.1073/pnas.1712396114

847 Scheller, N., Resa-Infante, P., de la Luna, S., Galao, R. P., Albrecht, M., Kaestner, L., . . . Diez, J. (2007).
848 Identification of PatL1, a human homolog to yeast P body component Pat1. *Biochim Biophys Acta,*
849 *1773*(12), 1786-1792. doi:10.1016/j.bbamcr.2007.08.009

850 Schwartz, D. C., & Parker, R. (1999). Mutations in translation initiation factors lead to increased rates
851 of deadenylation and decapping of mRNAs in Saccharomyces cerevisiae. *Mol Cell Biol, 19*(8), 5247-
852 5256.

853 Schwartz, D. C., & Parker, R. (2000). mRNA decapping in yeast requires dissociation of the cap binding
854 protein, eukaryotic translation initiation factor 4E. *Mol Cell Biol, 20*(21), 7933-7942.

855 Seydoux, G., & Braun, R. E. (2006). Pathway to totipotency: lessons from germ cells. *Cell, 127*(5), 891-
856 904. doi:10.1016/j.cell.2006.11.016

857 Shah, K. H., Zhang, B., Ramachandran, V., & Herman, P. K. (2013). Processing body and stress granule
858 assembly occur by independent and differentially regulated pathways in Saccharomyces cerevisiae.
859 *Genetics, 193*(1), 109-123. doi:10.1534/genetics.112.146993

860 Sharif, H., Ozgur, S., Sharma, K., Basquin, C., Urlaub, H., & Conti, E. (2013). Structural analysis of the
861 yeast Dhh1-Pat1 complex reveals how Dhh1 engages Pat1, Edc3 and RNA in mutually exclusive
862 interactions. *Nucleic Acids Res, 41*(17), 8377-8390. doi:10.1093/nar/gkt600

863 Sheth, U., & Parker, R. (2003). Decapping and decay of messenger RNA occur in cytoplasmic processing
864 bodies. *Science, 300*(5620), 805-808. doi:10.1126/science.1082320

865 Sun, M., Schwalb, B., Schulz, D., Pirkl, N., Etzold, S., Lariviere, L., . . . Cramer, P. (2012). Comparative
866 dynamic transcriptome analysis (cDTA) reveals mutual feedback between mRNA synthesis and
867 degradation. *Genome Res, 22*(7), 1350-1359. doi:10.1101/gr.130161.111

868 Teixeira, D., Sheth, U., Valencia-Sanchez, M. A., Brengues, M., & Parker, R. (2005). Processing bodies
869 require RNA for assembly and contain nontranslating mRNAs. *Rna, 11*(4), 371-382.
870 doi:10.1261/rna.7258505

871 Tucker, M., Staples, R. R., Valencia-Sanchez, M. A., Muhlrad, D., & Parker, R. (2002). Ccr4p is the
872 catalytic subunit of a Ccr4p/Pop2p/Notp mRNA deadenylase complex in Saccharomyces cerevisiae.
873 *Embo j, 21*(6), 1427-1436. doi:10.1093/emboj/21.6.1427

874 Vallotton, P., van Oijen, A. M., Whitchurch, C. B., Gelfand, V., Yeo, L., Tsiavaliaris, G., . . . Grunwald, D.
875 (2017). Diatrack particle tracking software: Review of applications and performance evaluation. *Traffic,*
876 *18*(12), 840-852. doi:10.1111/tra.12530

877

878

Figure 1

A.

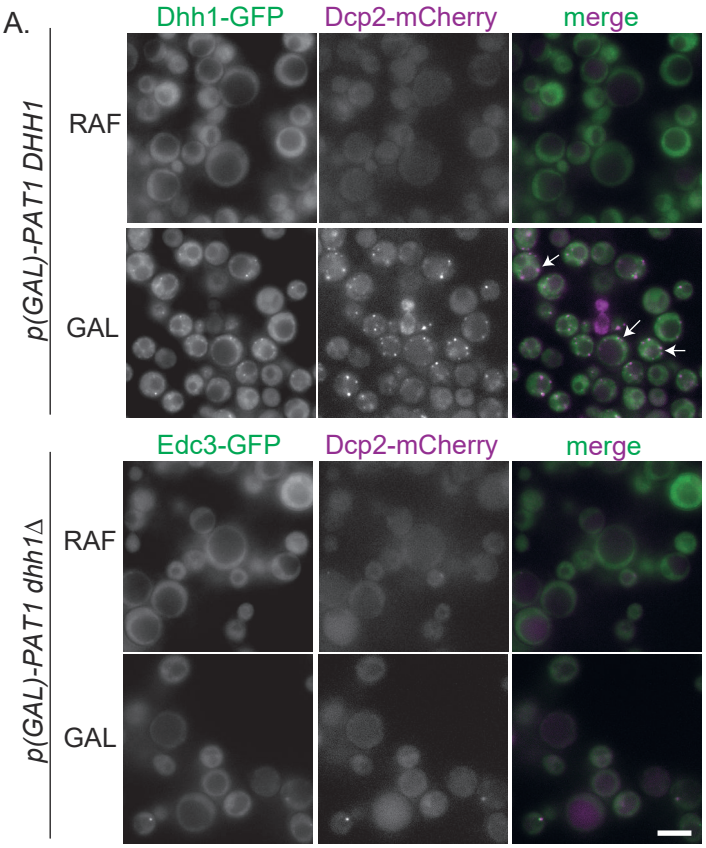

B.

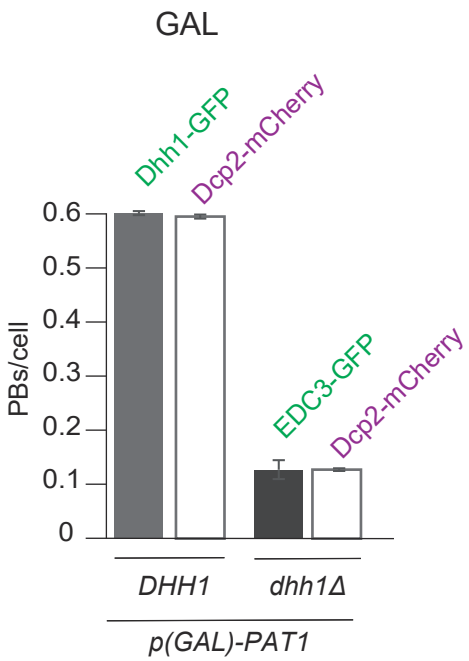

C.

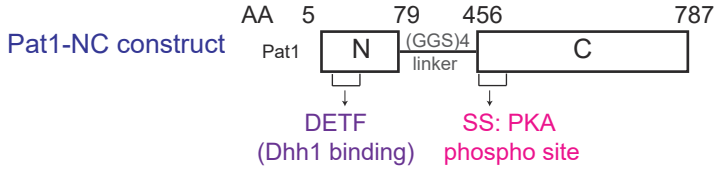

D.

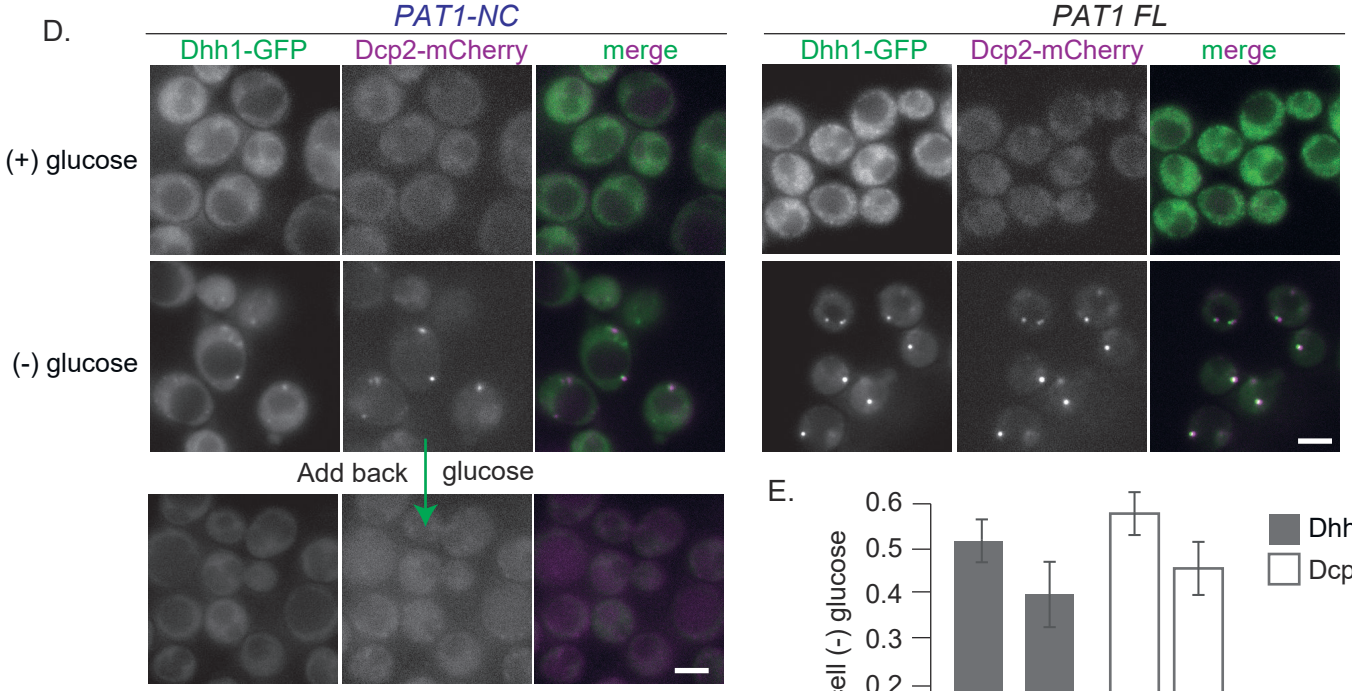

E.

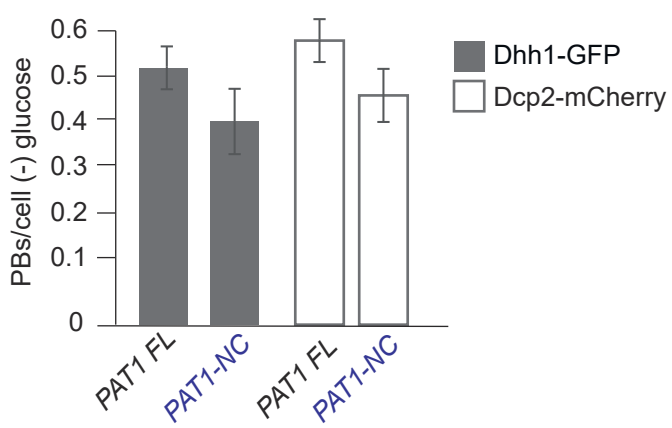

F.

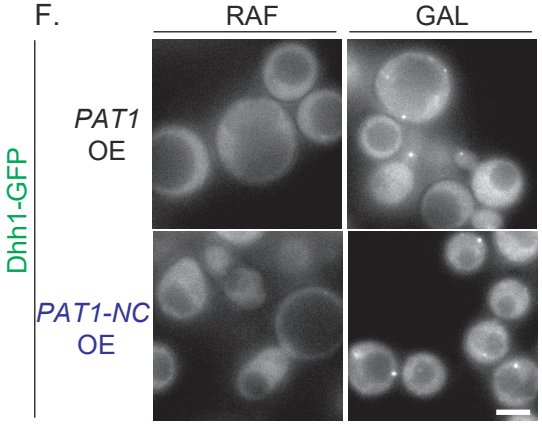

G.

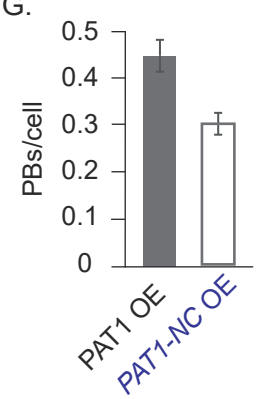

Figure S1

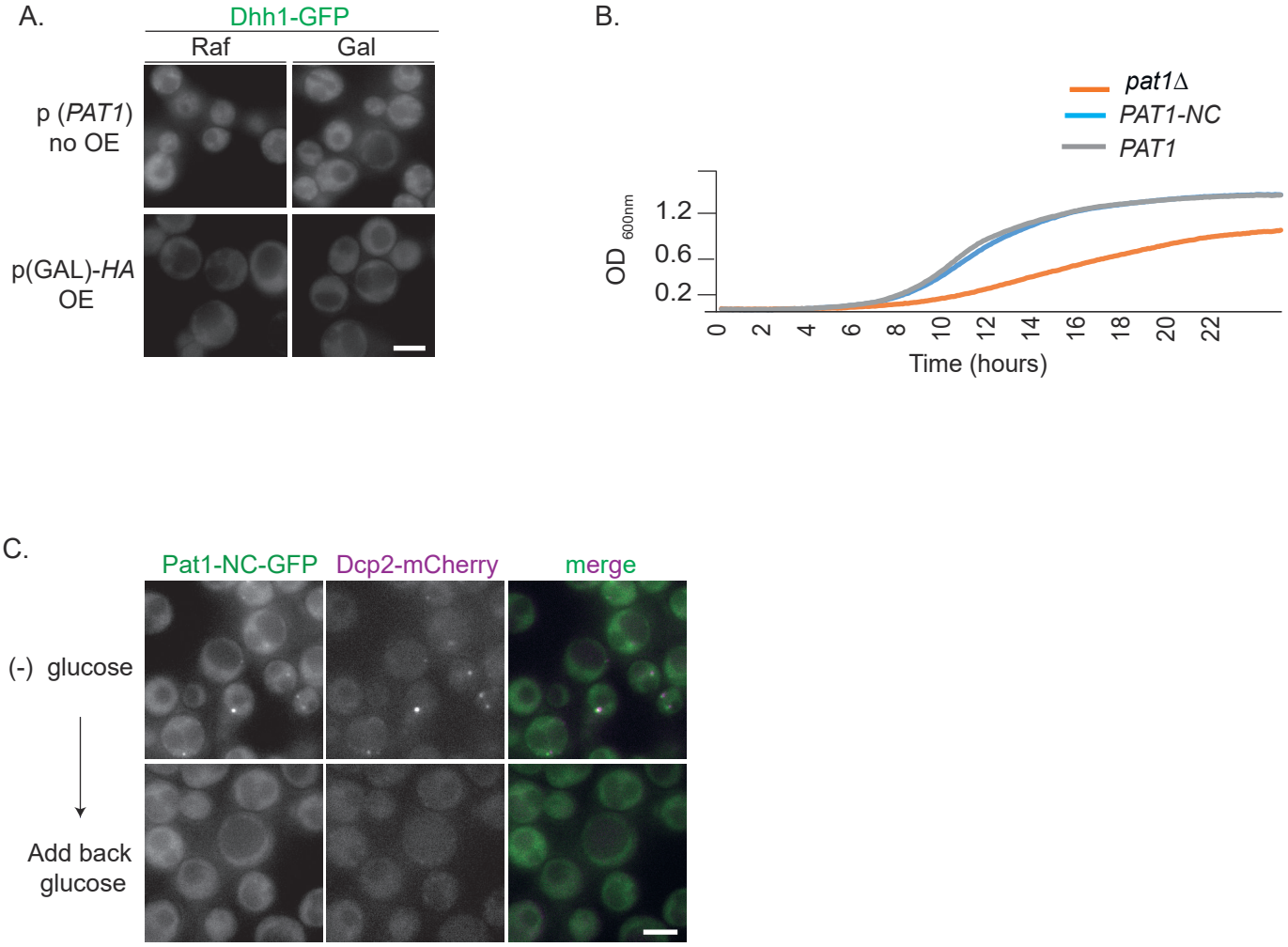
A.
Dhh1-GFP
Raf
Gal
p (PAT1) no OE
p(GAL)-HA OE
B.
pat1Δ
PAT1-NC
PAT1
OD 600nm
1.2
0.6
0.2
0
2
4
6
8
10
12
14
16
18
20
22
Time (hours)
C.
Pat1-NC-GFP
Dcp2-mCherry
merge
(-) glucose
Add back glucose

Figure 2

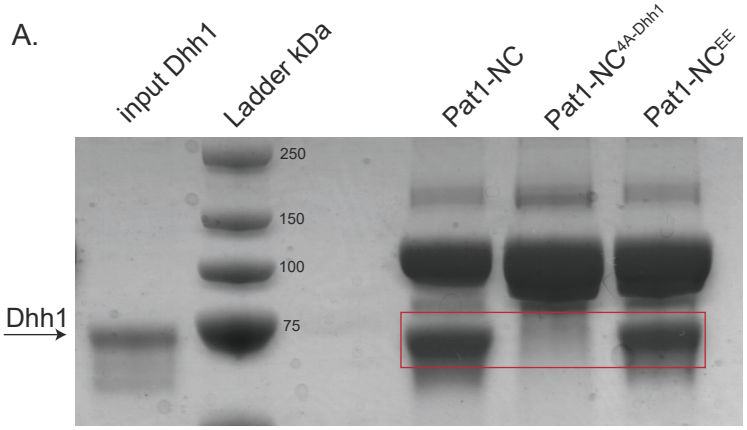
A.
input Dhh1
Ladder kDa
Pat1-NC
Pat1-NC4A-Dhh1
Pat1-NCEE
250
150
100
75
Dhh1

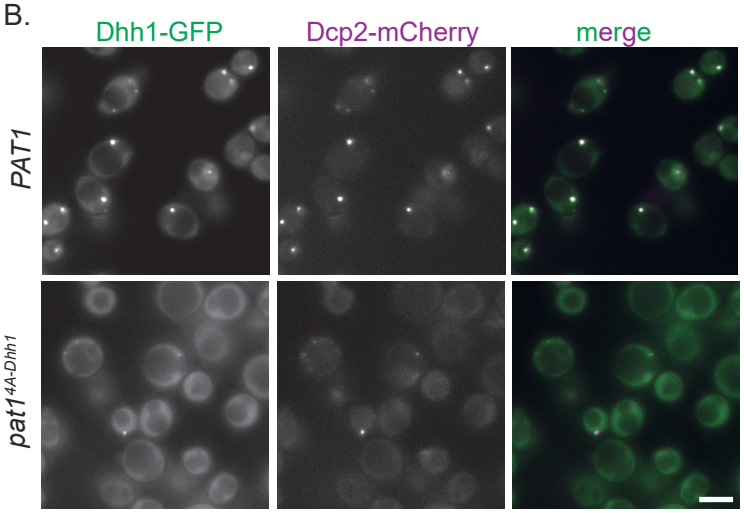
B.
Dhh1-GFP
Dcp2-mCherry
merge
PAT1
pat14A-Dhh1

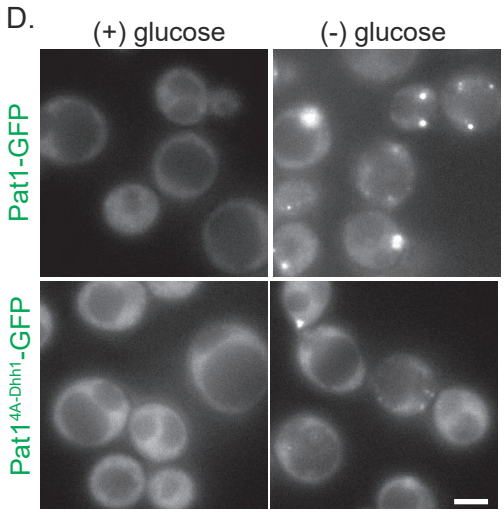
D.
(+) glucose
(-) glucose
Pat1-GFP
Pat14A-Dhh1-GFP

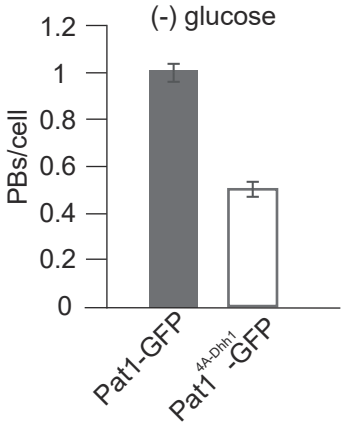
E.
(-) glucose
PBs/cell
1.2
1
0.8
0.6
0.4
0.2
0
Pat1-GFP
Pat14A-Dhh1-GFP

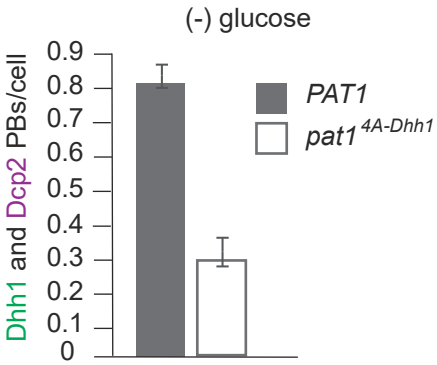
C.
(-) glucose
Dhh1 and Dcp2 PBs/cell
0.9
0.8
0.7
0.6
0.5
0.4
0.3
0.2
0.1
0
PAT1
pat14A-Dhh1

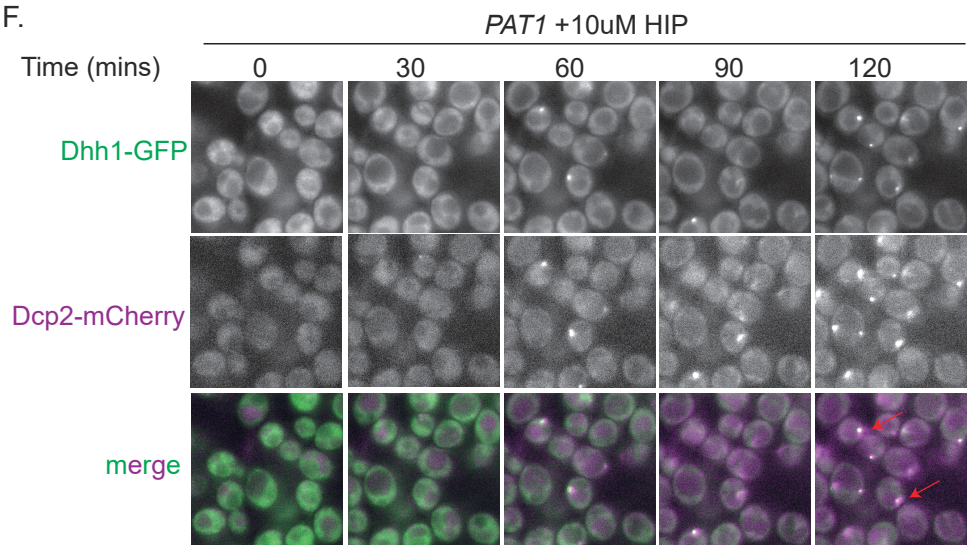
F.
PAT1 +10uM HIP
Time (mins)
0
30
60
90
120
Dhh1-GFP
Dcp2-mCherry
merge

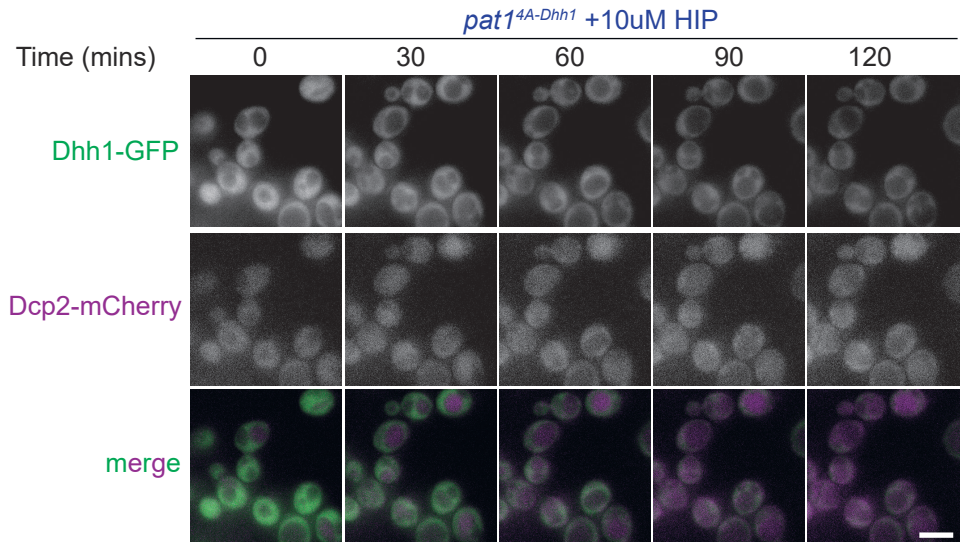
pat14A-Dhh1 +10uM HIP
Time (mins)
0
30
60
90
120
Dhh1-GFP
Dcp2-mCherry
merge

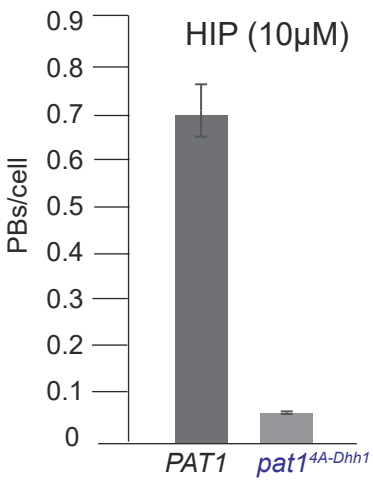
HIP (10μM)
PBs/cell
0.9
0.8
0.7
0.6
0.5
0.4
0.3
0.2
0.1
0
PAT1
pat14A-Dhh1

Figure S2

A.

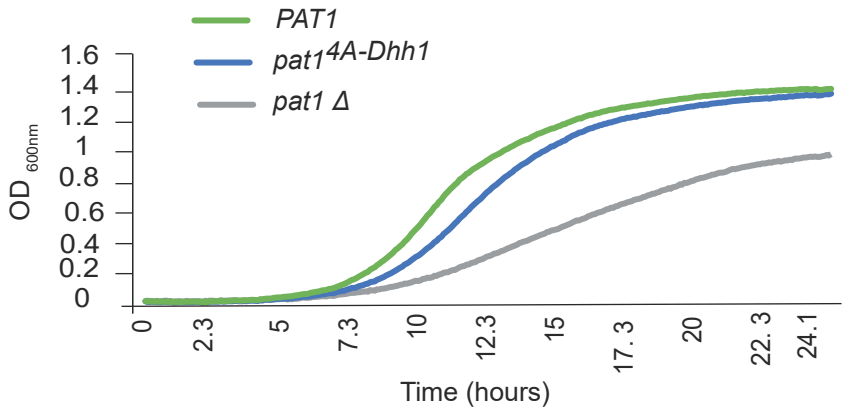
PAT1
pat1 4A-Dhh1
pat1 Δ
OD 600nm
1.6
1.4
1.2
1
0.8
0.6
0.4
0.2
0
0
2.3
5
7.3
10
12.3
15
17. 3
20
22. 3
24.1
Time (hours)

B.

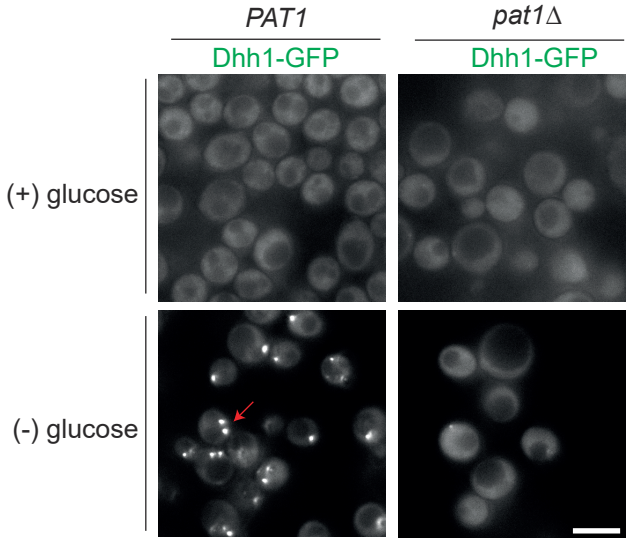
PAT1
pat1Δ
Dhh1-GFP
Dhh1-GFP
(+) glucose
(-) glucose

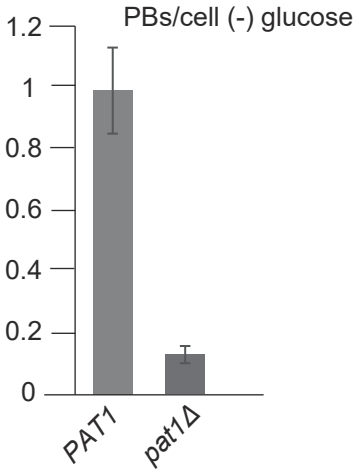
PBs/cell (-) glucose
1.2
1
0.8
0.6
0.4
0.2
0
PAT1
pat1Δ

Figure 3

A.

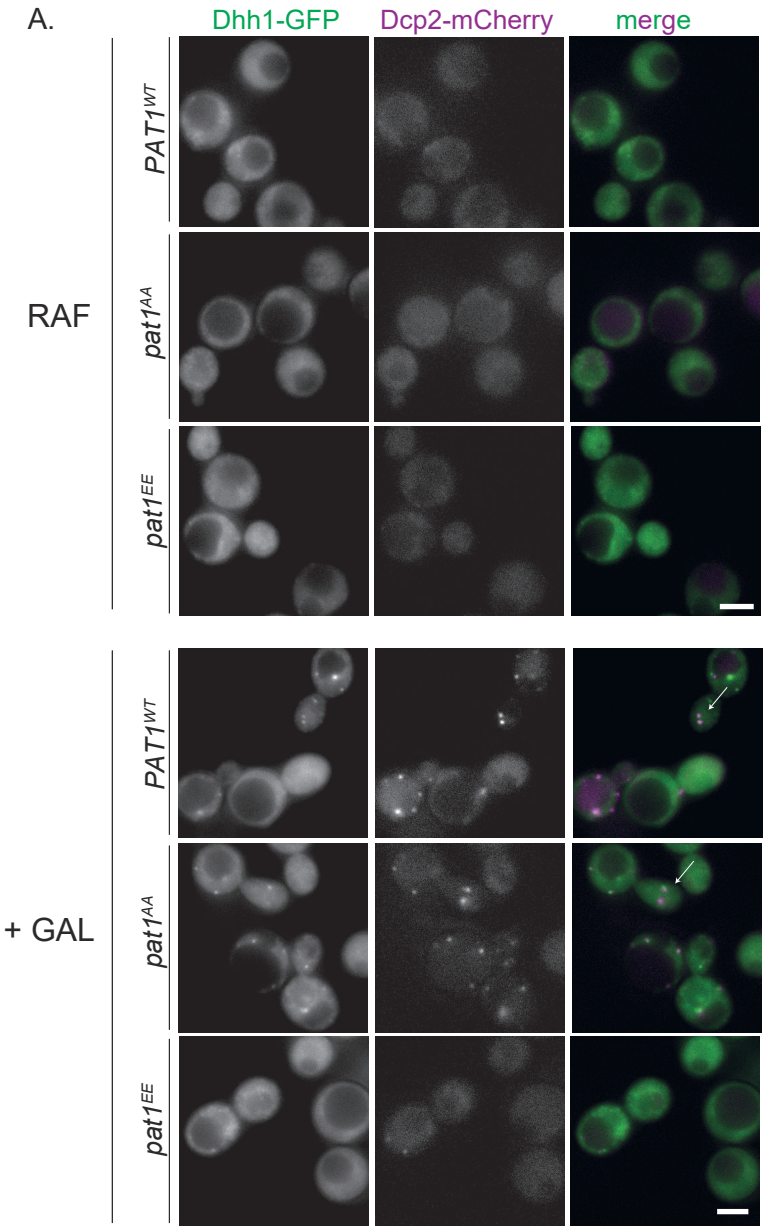

B.

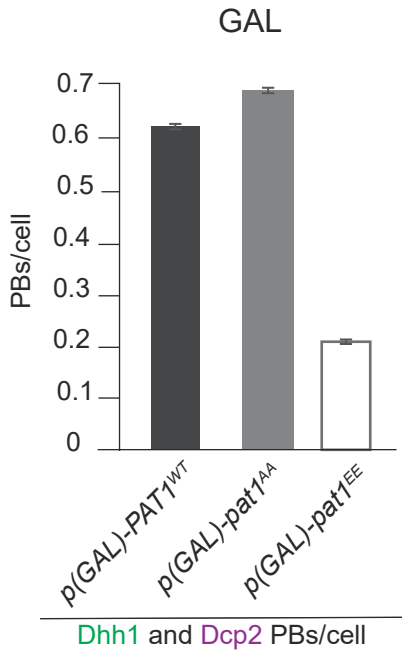

C.

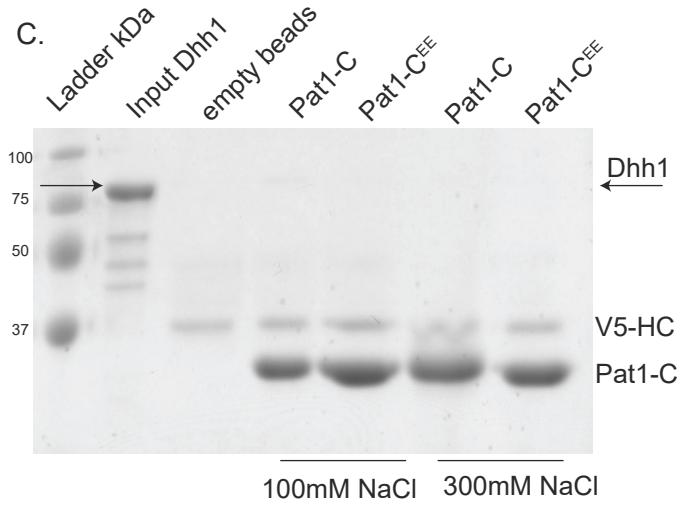

D.

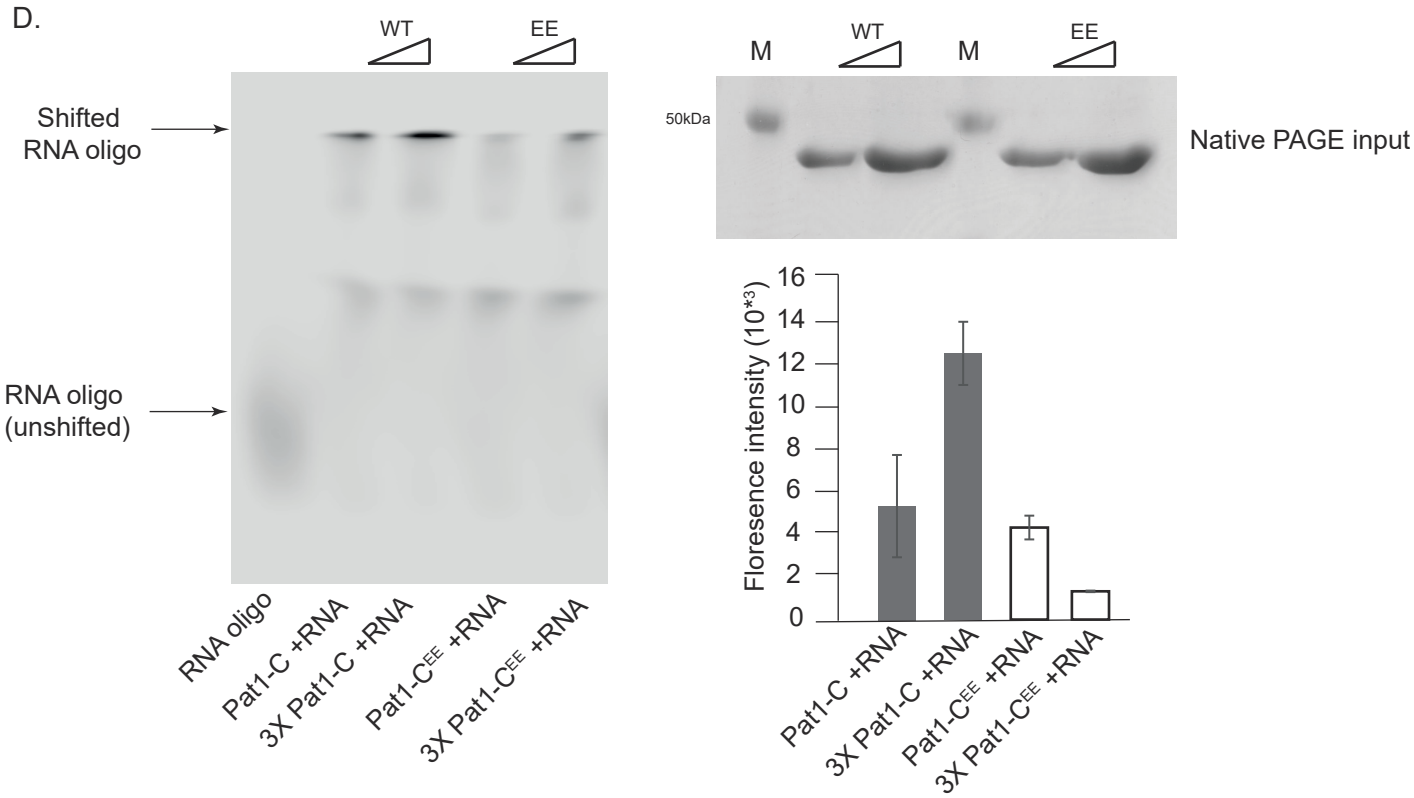

Figure S3

A.

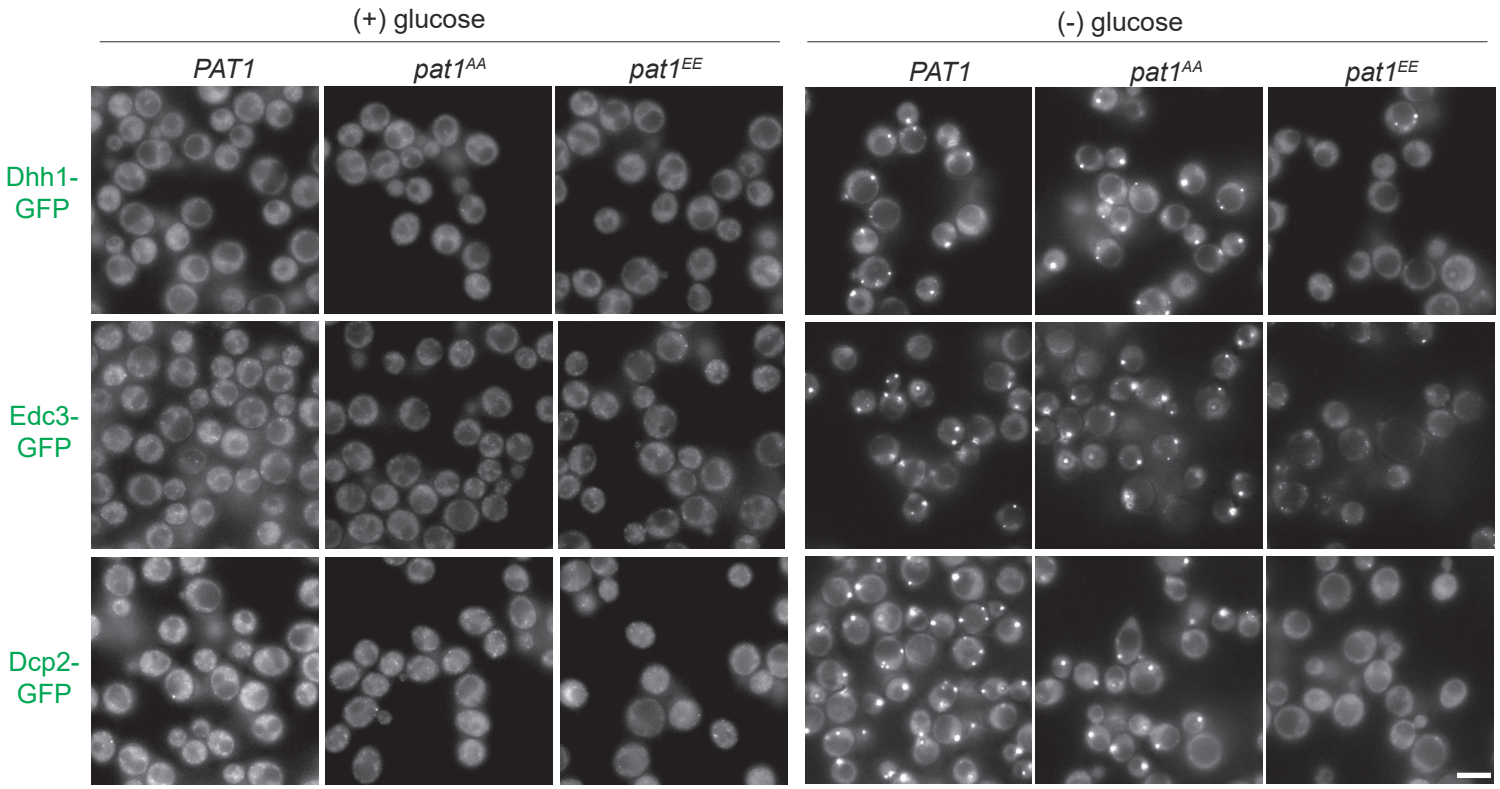
(+) glucose
(-) glucose
PAT1
pat1AA
pat1EE
PAT1
pat1AA
pat1EE
Dhh1-GFP
Edc3-GFP
Dcp2-GFP

B.

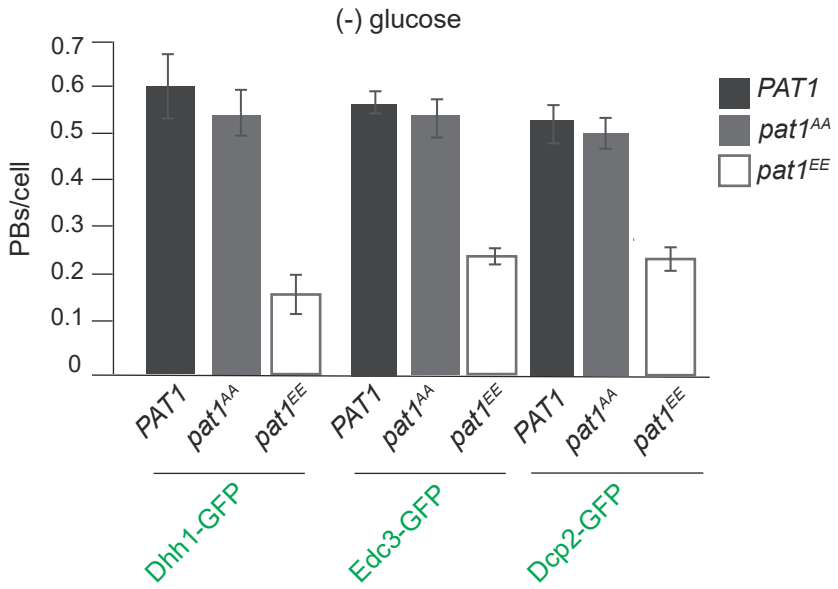
(-) glucose
PBs/cell
0.7
0.6
0.5
0.4
0.3
0.2
0.1
0
PAT1
pat1AA
pat1EE
PAT1
pat1AA
pat1EE
PAT1
pat1AA
pat1EE
Dhh1-GFP
Edc3-GFP
Dcp2-GFP

Figure 4

A.

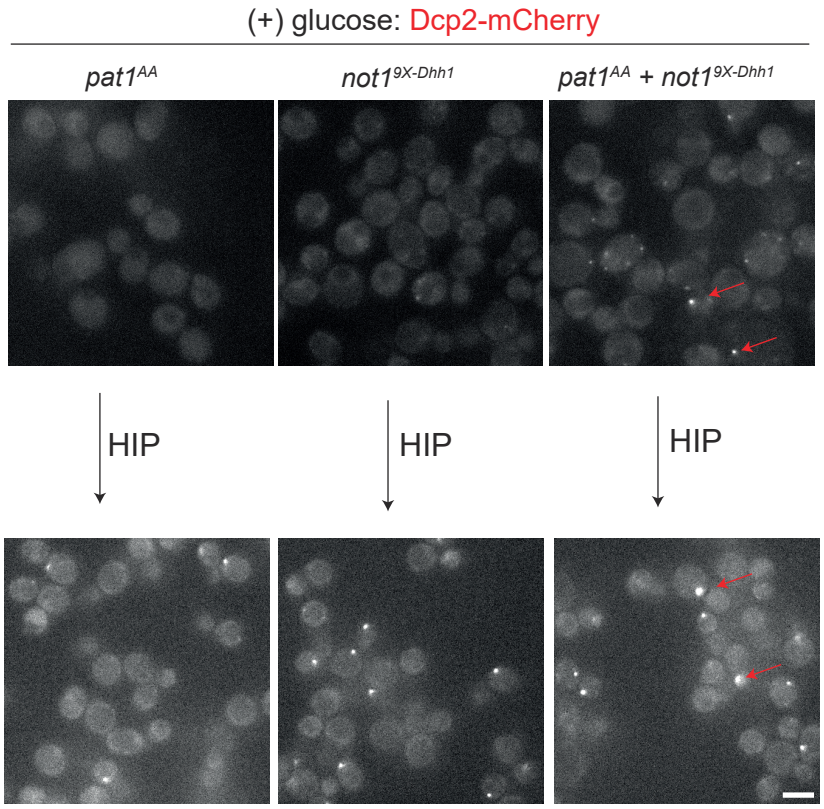
(+) glucose: Dcp2-mCherry
pat1AA
not19X-Dhh1
pat1AA + not19X-Dhh1
HIP
HIP
HIP

B.

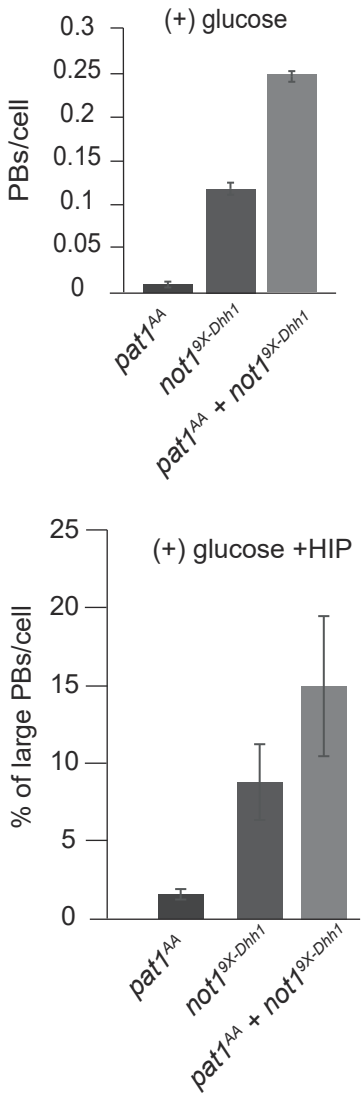
(+) glucose
PBs/cell
0.3
0.25
0.2
0.15
0.1
0.05
0
pat1AA
not19X-Dhh1
pat1AA + not19X-Dhh1
(+) glucose +HIP
% of large PBs/cell
25
20
15
10
5
0
pat1AA
not19X-Dhh1
pat1AA + not19X-Dhh1

Figure S4

A.

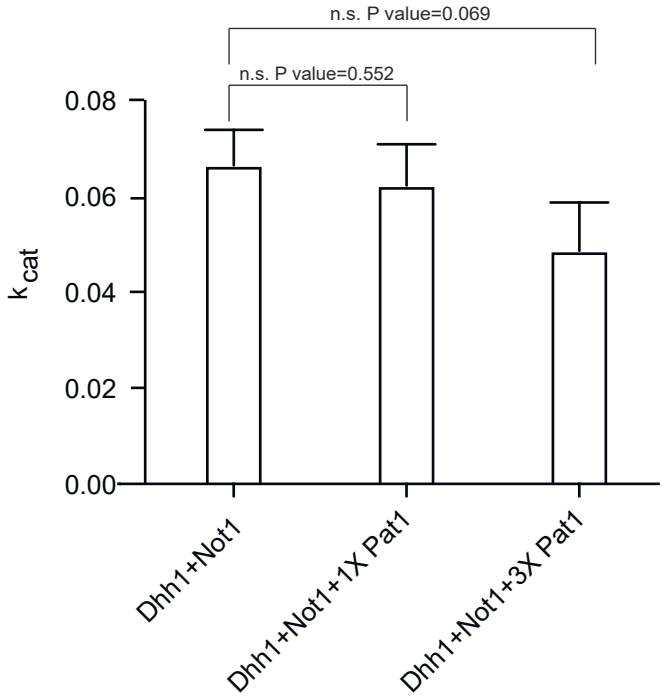

B.

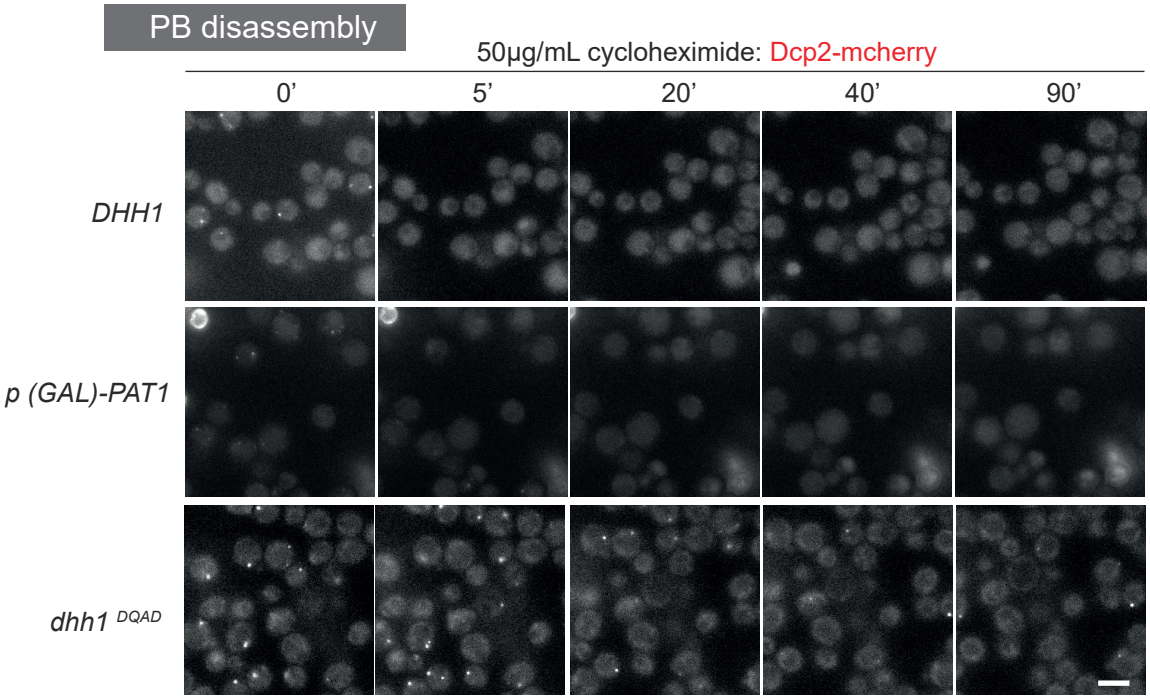

C.

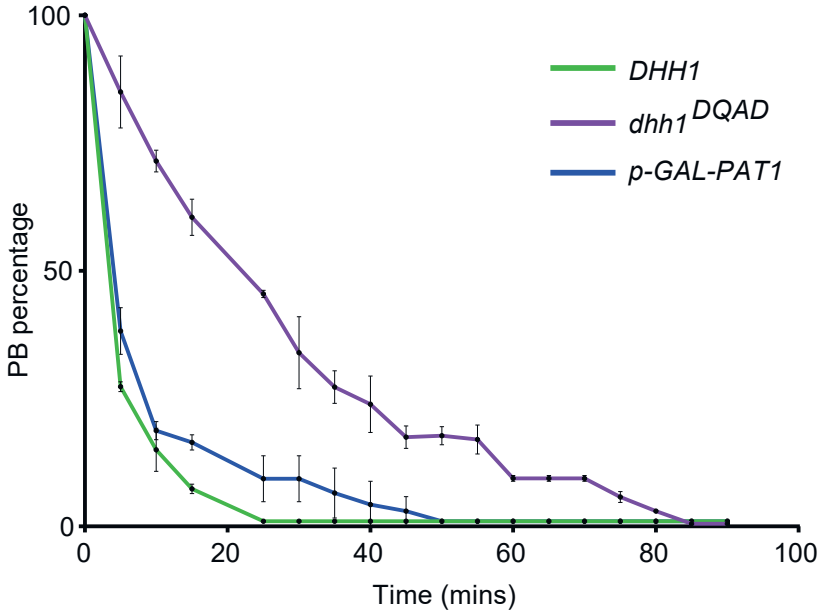

Figure 5

A.

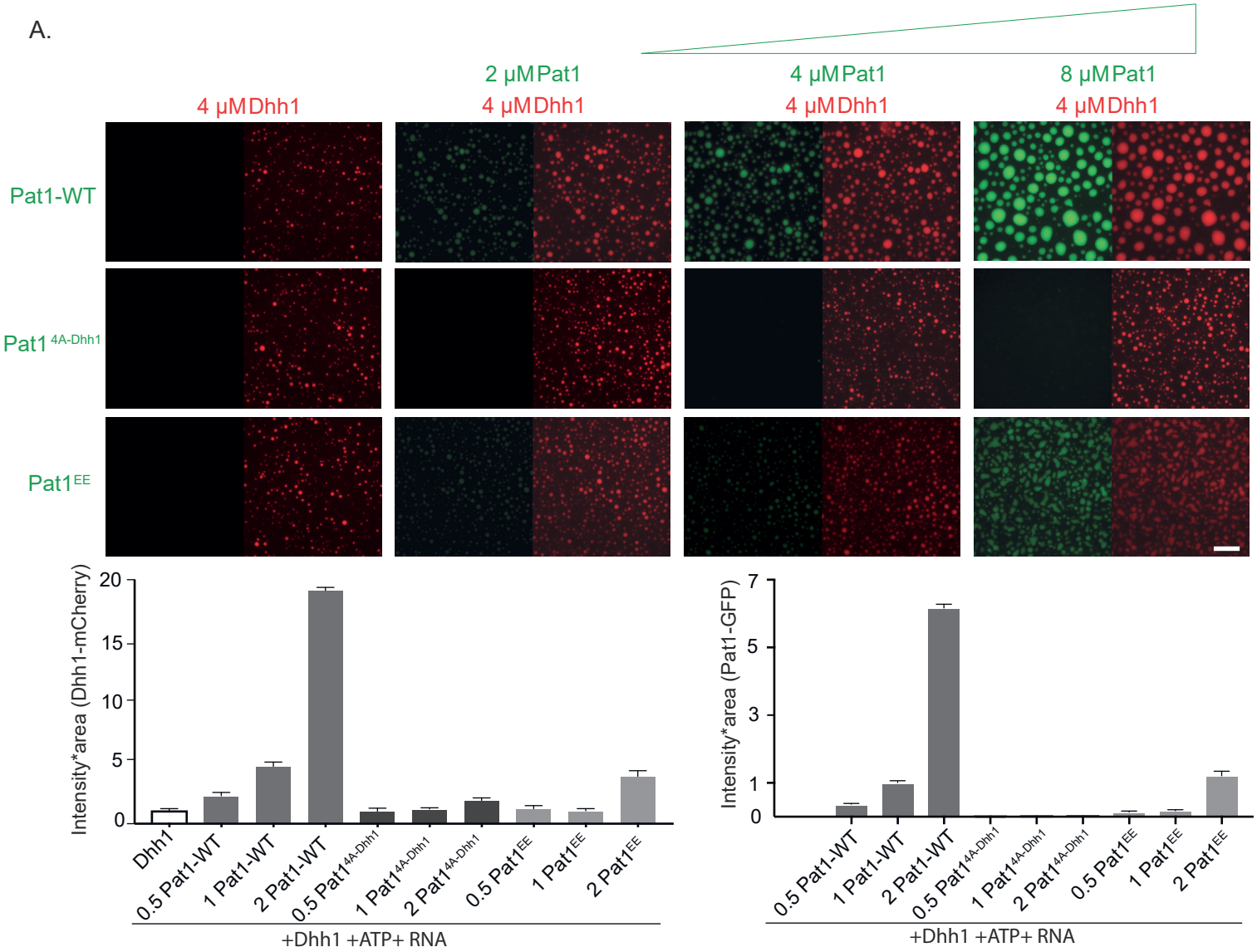
2 μM Pat1
4 μM Pat1
8 μM Pat1
4 μM Dhh1
4 μM Dhh1
4 μM Dhh1
4 μM Dhh1
Pat1-WT
Pat1 4A-Dhh1
Pat1 EE
Intensity*area (Dhh1-mCherry)
Intensity*area (Pat1-GFP)
Dhh1
0.5 Pat1-WT
1 Pat1-WT
2 Pat1-WT
0.5 Pat1 4A-Dhh1
1 Pat1 4A-Dhh1
2 Pat1 4A-Dhh1
0.5 Pat1 EE
1 Pat1 EE
2 Pat1 EE
+Dhh1 +ATP+ RNA

B.

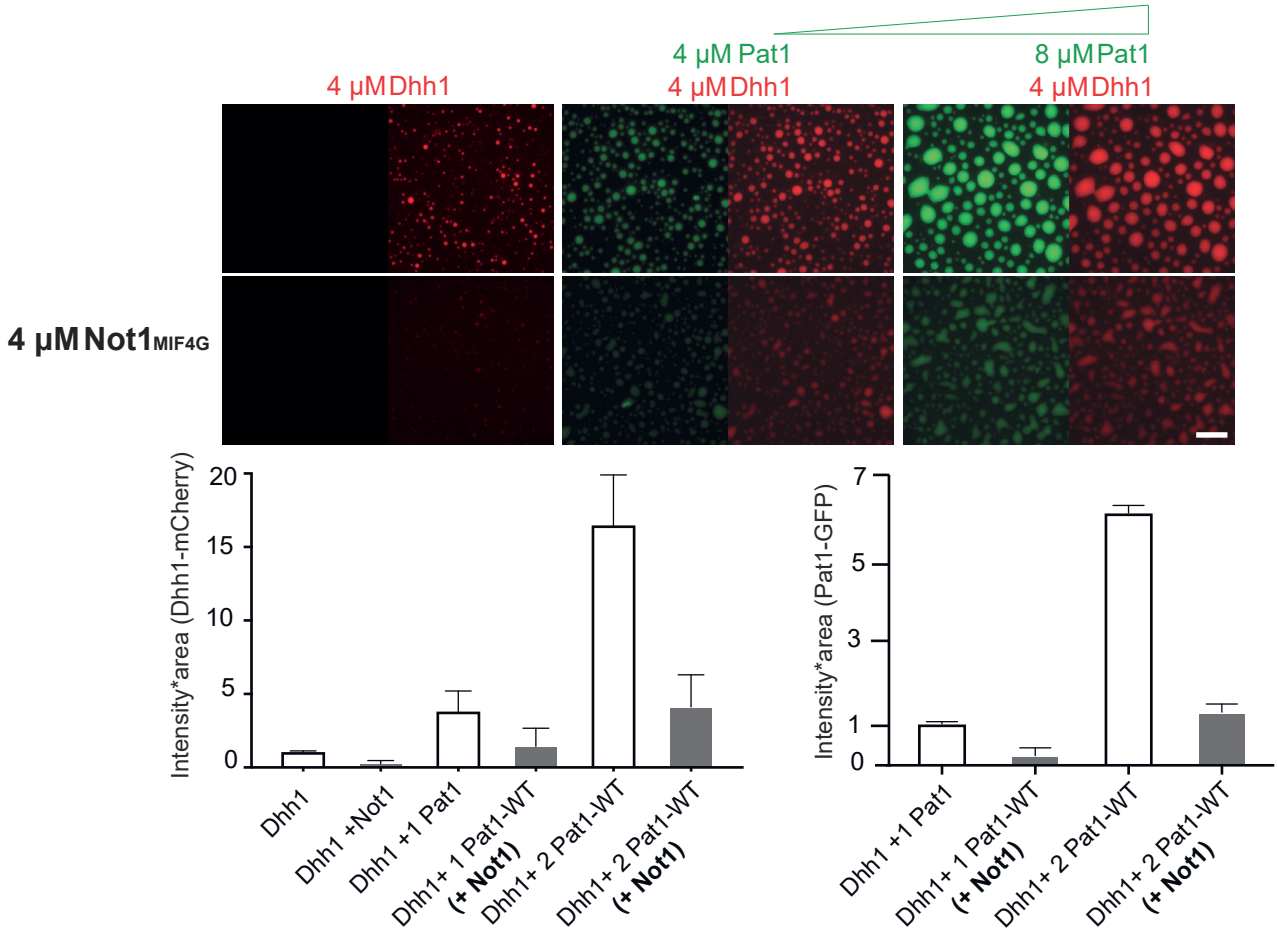
4 μM Pat1
8 μM Pat1
4 μM Dhh1
4 μM Dhh1
4 μM Dhh1
4 μM Not1MIF4G
Intensity*area (Dhh1-mCherry)
Intensity*area (Pat1-GFP)
Dhh1
Dhh1 +Not1
Dhh1 +1 Pat1
Dhh1+ 1 Pat1-WT (+ Not1)
Dhh1+ 2 Pat1-WT
Dhh1+ 2 Pat1-WT (+ Not1)

Figure S5

A.

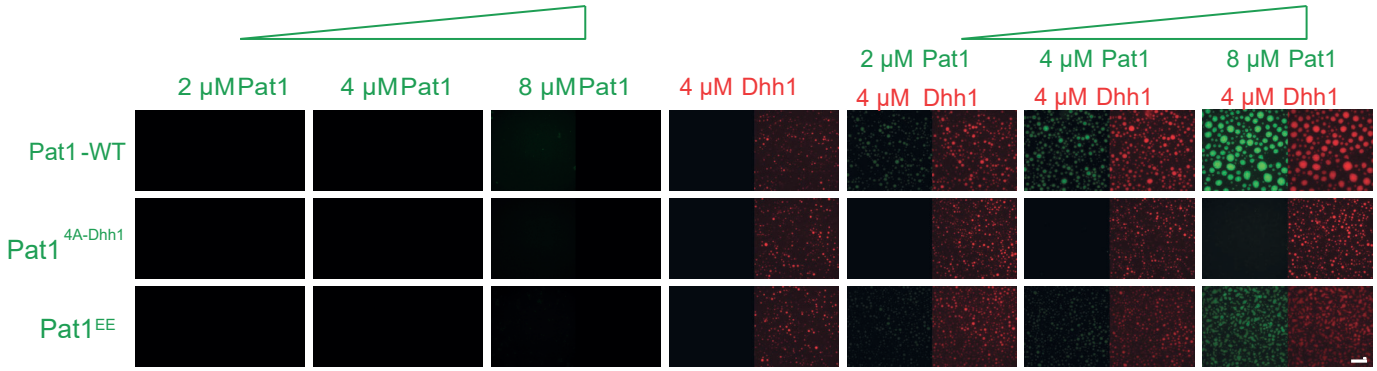
2 μM Pat1
4 μM Pat1
8 μM Pat1
4 μM Dhh1
2 μM Pat1
4 μM Dhh1
4 μM Pat1
4 μM Dhh1
8 μM Pat1
4 μM Dhh1
Pat1-WT
Pat1 4A-Dhh1
Pat1 EE

Figure 6

A.

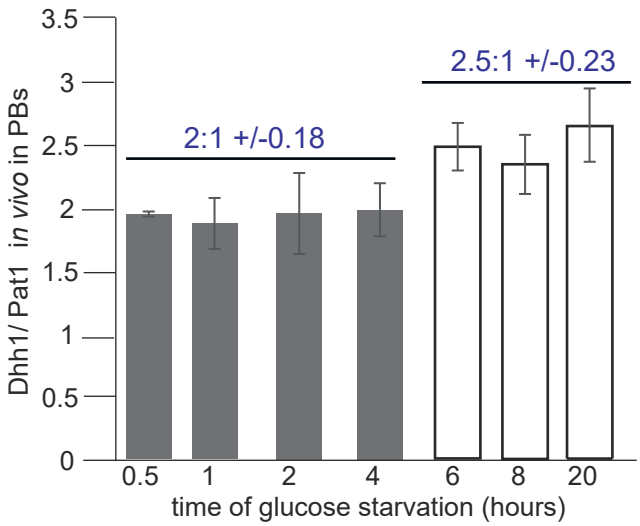

B.

Stoichiometry of Dhh1/Pat1 in *in vitro* LLPS droplets

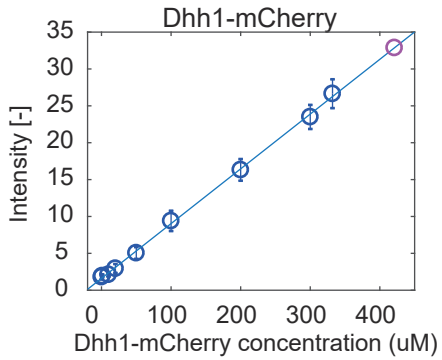

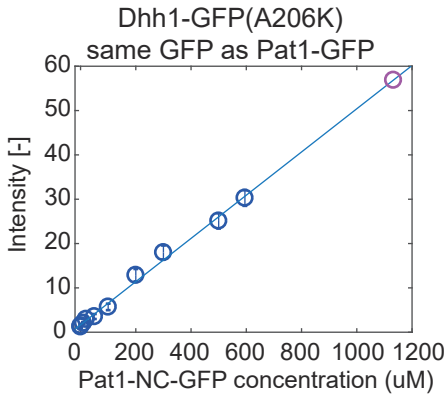

2 μM Dhh1, 5 mM ATP, 0.1 mg/ml pU

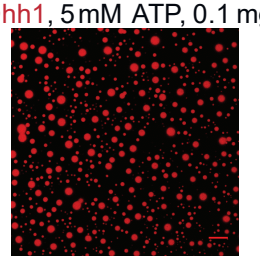

2 μM Dhh1, 5 mM ATP, 0.1 mg/ml pU + 4uM Pat1

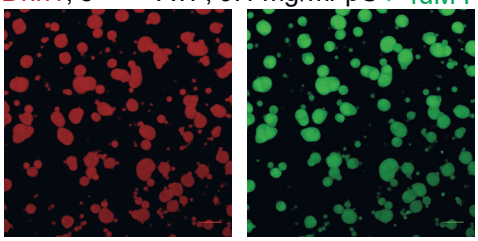

Dhh1:Pat1 in *in vitro* droplets= 2.7:1+/- 0.13

C.

Tug of war model between Pat1 and Not1 to promote PB assembly and Disassembly respectively

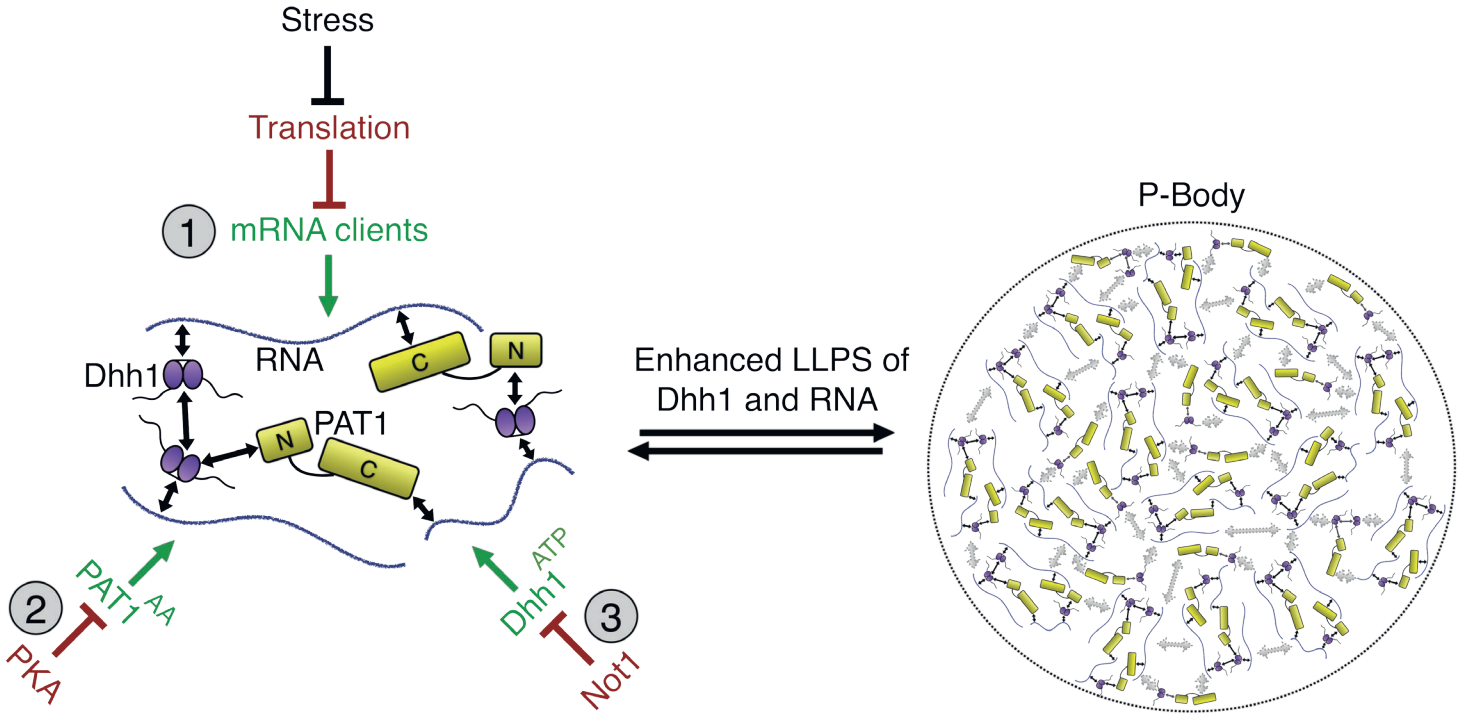

Figure S6

A.

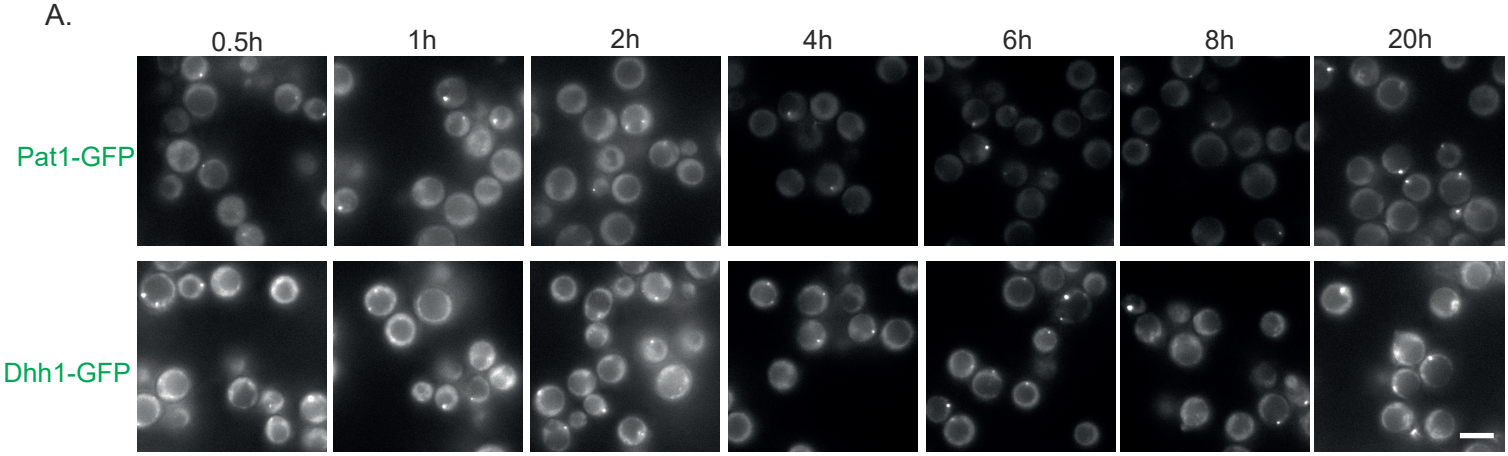

B.

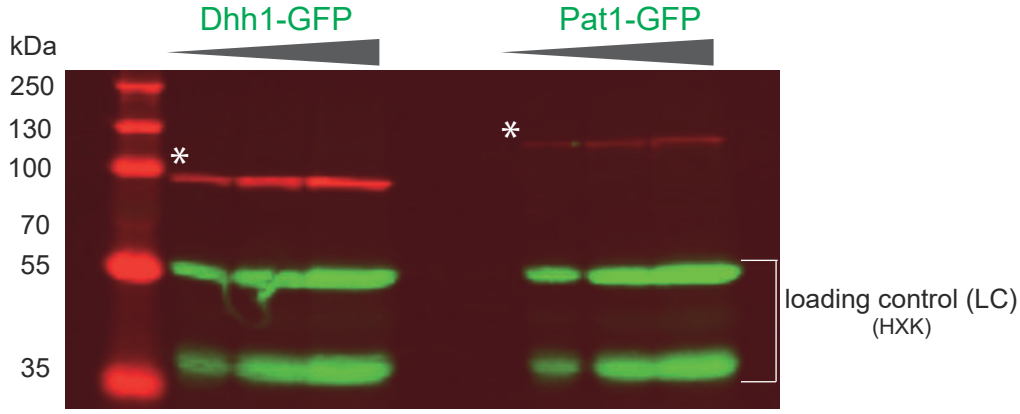

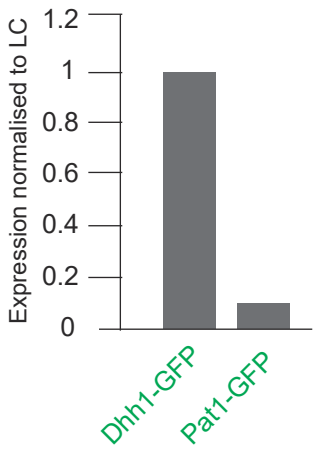

C.

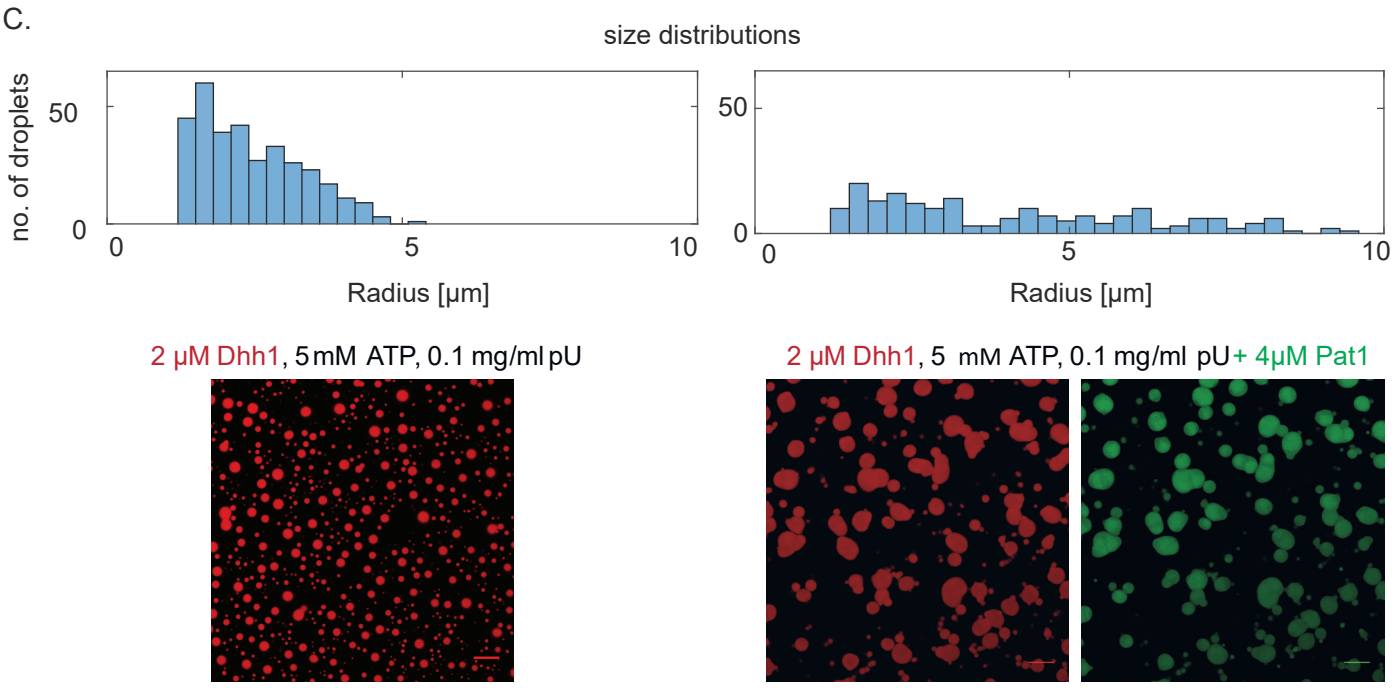

Figure S7

A.

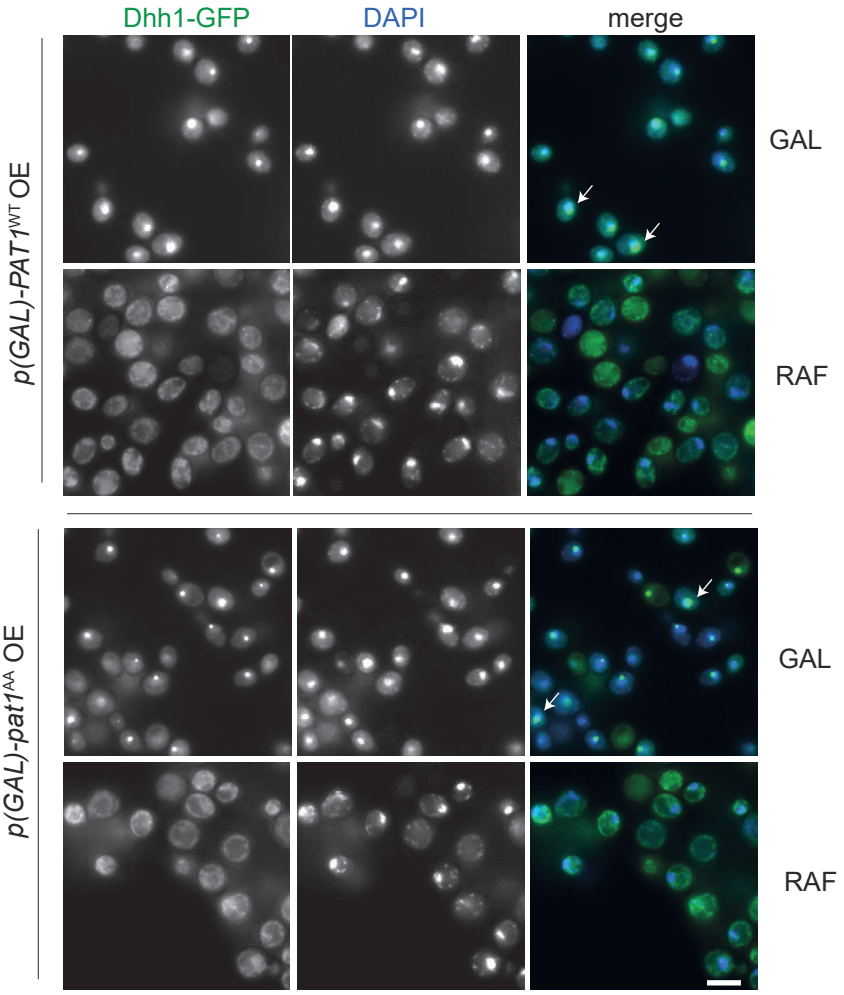

B.

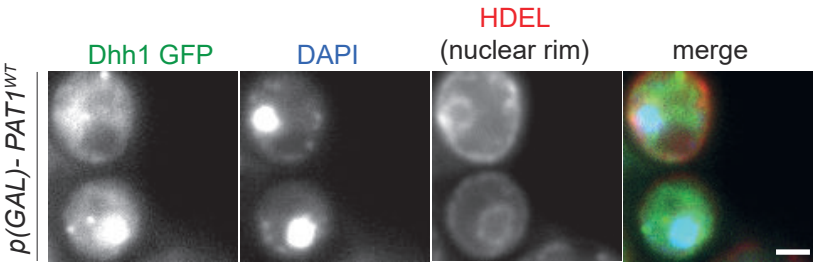
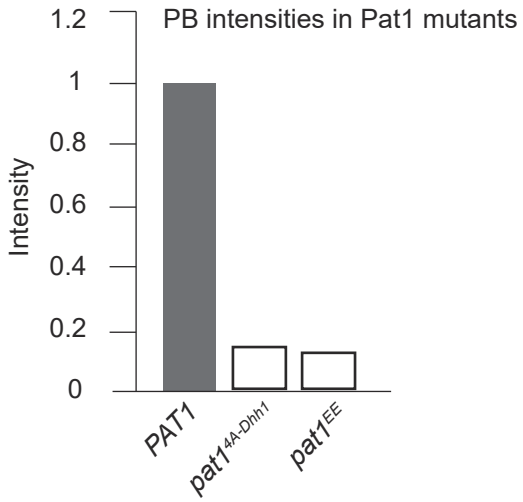
C.